The relationship between cloud condensation nuclei (CCN) concentration and light extinction of dried particles: indications of underlying aerosol processes and implications for satellite-based CCN estimates

Y. Shinozuka[1,2], A.D. Clarke[3], A. Nenes[4,5], A. Jefferson[6,7], R. Wood[8], C.S. McNaughton[3,9], J. Ström[10], P. Tunved[10], J. Redemann[11], K.L. Thornhill[12], R.H. Moore[13], T.L. Lathem[4,14], J.J. Lin[4], Y.J. Yoon[15]

[1] NASA Ames Research Center Cooperative for Research in Earth Science and Technology, Moffett Field, California, USA

[2] Bay Area Environmental Research Institute, Petaluma, California, USA

[3] School of Ocean and Earth Science and Technology, University of Hawaii, Honolulu, Hawaii, USA

[4] School of Earth and Atmospheric Sciences, Georgia Institute of Technology, Atlanta, Georgia, USA

[5] School of Chemical and Biomolecular Engineering, Georgia Institute of Technology, Atlanta, Georgia, USA

[6] Cooperative Institute for Research in Environmental Science (CIRES), University of Colorado, Boulder, Colorado, USA

[7] NOAA Earth System Research Laboratory, Boulder, Colorado, USA

[8] Department of Atmospheric Sciences, University of Washington, Seattle, Washington, USA

[9] Golder Associates Ltd., Saskatoon, Saskatchewan, Canada

[10] Department of Applied Environmental Science, Stockholm University, Sweden

[11] NASA Ames Research Center, Moffett Field, California, USA

[12] Science Systems and Applications Inc., Hampton, Virginia, USA

[13] NASA Langley Research Center, Hampton, Virginia, USA

[14] Phillips 66 Research Center, Bartlesville, Oklahoma, USA

[15] Korea Polar Research Institute, Yeonsu-Gu, Incheon, Korea

Correspondence to: Y. Shinozuka (Yohei.Shinozuka@nasa.gov)

Abstract

We examine the relationship between the number concentration of boundary-layer cloud condensation nuclei (CCN) and light extinction to investigate underlying aerosol processes and satellite-based CCN estimates. For a variety of airborne and ground-based observations not dominated by dust, regression identifies the CCN (cm^{-3}) at 0.4±0.1% supersaturation with $10^{0.3\alpha+1.3}\sigma^{0.75}$ where σ (Mm^{-1}) is the 500 nm extinction coefficient by dried particles and α is the Angstrom exponent. The deviation of one-kilometer horizontal average data from this approximation is typically within a factor of 2.0. $\partial\log CCN/\partial\log\sigma$ is less than unity because, among other explanations, growth processes generally make aerosols scatter more light without increasing their number. This, barring special meteorology-aerosol connections, associates a doubling of aerosol optical depth with less than a doubling of CCN, contrary to previous studies based on heavily averaged measurements or a satellite algorithm.

1 Introduction

Aerosol-cloud interactions (ACI) are the largest source of uncertainty in estimates of radiative forcing responsible for the on-going climate change (Boucher et al., 2013). ACI for warm clouds depend on the number concentration of cloud condensation nuclei (CCN), the particles capable of initiating drop formation at a given supersaturation (Pruppacher and Klett, 1980), not on aerosol optical properties. Yet, aerosol optical depth (AOD) and its variants weighted by the spectral dependence over visible and near infrared (VNIR) wavelengths are commonly substituted for CCN in ACI studies (see below for examples). The substitution is motivated by the wide availability in space and time of satellite retrievals, an advantage over the sparse

CCN measurements. But underlying assumptions on the relationship between CCN and VNIR AOD remain to be examined with direct observations over a horizontal resolution relevant to common clouds (e.g., near one kilometer).

The CCN-AOD relationship is complicated partly because these quantities refer to different volumes of air. Whereas the CCN most relevant to ACI are located at the cloud base altitude, the AOD is defined for the entire vertical column. Aerosols at other altitudes contribute to it but not to the CCN. The air mass interacting with clouds may be kilometers away from, or hours after, clear-sky satellite measurements of AOD, and may have finer horizontal and temporal resolution. These differences matter because aerosol spatio-temporal distribution is generally inhomogeneous.

Even the CCN-extinction relationship at a given location and time is complicated, as each of these quantities depends on particle size and hygroscopicity in its own convoluted way. Most CCN are in the Aitken mode and the smaller sizes of the accumulation mode, the exact lower limit depending on the hygroscopicity. That is because particles are typically most numerous in these size ranges (Seinfeld and Pandis, 2006) and because the critical dry diameter for droplet activation at a supersaturation of 0.2-0.6% is usually 50-120 nm (Pringle et al., 2010). The light extinction at midvisible wavelengths is normally dominated by the accumulation or coarse mode where both particle volume and scattering efficiency are greater than for smaller sizes (Waggoner et al., 1981). Particles that are relatively small may grow into optically active sizes at high ambient relative humidity (RH) due to uptake of water. As a result, particles near 100 nm can add to the CCN number without significantly changing the light extinction, and the extinction can increase upon humidity rises without changing the CCN number. Other aerosol intensive properties such as refractive index, mixing state, particle shape and surface tension can also influence the relationship.

The CCN-AOD relationship has been approximated by several parameterizations, each based on either heavily averaged measurements or a satellite algorithm. Some of them are applied to satellite AOD products to study the aerosol effects on warm clouds. Virtually all existing parameterizations have $\partial \log CCN / \partial \log AOD$ of unity or greater, i.e., the CCN concentration at least doubles as AOD doubles. These parameterizations can be sorted into four groups.

The simplest CCN retrieval strategies scale CCN concentrations with AOD at a single wavelength. They implicitly assume negligible variability in the combination of aerosol spatio-temporal distribution and intensive properties. Andreae (2009) finds from dozens of

field experiments that, on an experiment average basis, AOD at 500 nm is correlated to CCN concentration at 0.4% supersaturation as $AOD_{500nm}=0.0027CCN_{0.4\%}^{0.640}$ with an R^2 of 0.88. There is about a factor-of-four range of CCN concentrations at a given AOD. The exponent 0.640 on CCN means that a doubling of AOD is associated with nearly a tripling of CCN. In an even simpler approach, Kaufman et al. (2005) use MODIS AOD as a surrogate for the concentration of the aerosols that interact with the cloud layer, i.e., $\partial\log CCN/\partial\log AOD=1$, to study the aerosol effect on shallow liquid clouds. Koren et al. (2008) employ the same technique to study aerosol effects on clouds over the Amazon, and Bellouin et al. (2013) to estimate the shortwave direct and first indirect radiative forcing of anthropogenic aerosols. Quaas et al. (2008) and Quaas et al. (2009) evaluate variously modeled aerosol effects in terms of their relationship with AOD. Their results indicate that global climate models generally overestimate the cloud albedo effect, though this, along with the effects on cloud droplet number concentration, liquid water path and other cloud properties, varies with the location and model.

Another prevalent strategy is to multiply a single-wavelength AOD by the Angstrom exponent, i.e., -1 times the slope of extinction spectrum in logarithmic scales. Nakajima et al. (2001) hypothesize that this product, now commonly called aerosol index (AI; not the TOMS/OMI aerosol index), is approximately proportional to the column aerosol number concentration (rather than CCN). Liu et al. (2011) examine the CCN-AI relationship directly using the observation over a polluted site in China. Bréon et al. (2002), Sekiguchi et al. (2003), Quaas et al. (2004) and Penner et al. (2012) study the relationship of AI with satellite-derived or modeled cloud microphysical properties. Penner et al. (2011) refer to model-simulated AOD and AI to evaluate the aerosol effects on cloud droplet number concentration (CDNC), leading to the conclusion that satellite methods underestimate the indirect climate forcing by aerosols. The assumptions behind these uses of AI are that the impact of particle size is partly accounted for by the Angstrom exponent and that the impact of spatio-temporal distribution and particle hygroscopicity is negligible. Importantly, AI is proportional to AOD for a constant Angstrom exponent, i.e., $\partial\log AI/\partial\log AOD=1$. Nakajima et al. (2001) mention that a more accurate proxy for column aerosol number is the AI raised to the power of 0.869 based on the AVHRR retrieval algorithm. This statement has been widely ignored by subsequent studies.

Another strategy relies on satellite-retrieved aerosol size distribution. Gassó and Hegg (2003) compute CCN concentration by three different methods. One of them relies on the MODIS over-ocean algorithm. The algorithm matches spectral radiance calculated from combinations of nine pre-set aerosol models to the spectral radiance observed over VNIR wavelengths by the space-borne sensor. This yields aerosol size distribution, among other products. The MODIS CCN product is the integral of the small-mode aerosol size distribution from a fixed radius of 30 nm (Appendix B of Remer et al. (2005), renamed PSML003_Ocean for MODIS Collection 6 (Levy et al., 2013)). This strategy, similar to the AI, accounts for the impact of particle size and refractive index only. The derived column-integral CCN concentration is proportional to the derived AOD. This product remains unvalidated and underutilized. Spectral fitting has been applied to ship-based columnar remote-sensing measurements as well (Sayer et al., 2012).

The study by Liu and Li (2014) is unique. Their analysis of five ground-based long-term measurements yields parameterizations that not only account for the size effect with Angstrom exponent. They also eliminate the impact of aerosol vertical distribution by referring to ground-level in situ optical measurements. The strategy should work with passive satellite observations of column AOD as input, as long as additional measurements or a transport model estimate the aerosol vertical profile. The impact of hygroscopicity is not directly accounted for, though they provide assessments on the changes in light scattering upon humidity changes and on single scattering albedo (SSA). The impact of horizontal-temporal distribution is obscured by the bin-averaging applied to a large number of CCN data. $\partial \log CCN / \partial \log \sigma_{sp} = 1.5178$ in their parameterization with the 450 nm scattering coefficient, σ_{sp}, for <80% ambient RH and SSA between 0.85 and 0.95. Jefferson (2010) also parameterizes the CCN concentration with ground-based optical observations; the use of backscattering fraction distinguishes her study from those mentioned above and the present study.

We propose a new parameterization between the CCN concentration and light extinction of dried particles, based on airborne and ground-based observations of aerosols at about one-kilometer horizontal resolutions. We also discuss underlying aerosol processes and satellite-based CCN estimates. This paper does not address advanced remote sensing capabilities such as angles, polarization and, setting aside a mention of its vertical resolution, lidar (Feingold and Grund, 1994; Ghan and Collins, 2004; Ghan et al., 2006; Müller et al., 2014; Veselovskii et al., 2002). This paper does not address pre-industrial era estimates either.

2 Methods

2.1 Experiments and Instruments

We use in situ aerosol measurements made aboard the NASA P-3 aircraft during the central Canada phase of ARCTAS (Jacob et al., 2010) and the California phase of DISCOVER-AQ from altitudes up to one kilometer, and ground-based long-term observations at several sites run by the US Department of Energy ARM program and Svalbard (Table 1). In addition, we use the AOD observed from the P-3 during ARCTAS Canada.

A solid diffuser inlet delivered ambient air to all the airborne in situ aerosol instruments. This inlet and sample plumbing pass aerosol with dry aerodynamic diameter at least up to 5.0 μm with better than 50% efficiency (McNaughton et al., 2007). The partial loss of coarse particles leads to an underestimate of light extinction, but its magnitude should be typically smaller than 15-25%, an estimate established for the NCAR Community Aerosol Inlet (Shinozuka et al., 2004) that passes fewer particles than do solid diffuser inlets (Huebert et al., 2004). The submicron particles that almost always dominate CCN are sampled isokinetically with a near 100% efficiency. The timing of the airborne records used in this study is adjusted by 7-10s, depending on the instrument and experiment, to account for the transport between the inlet tip and the instrument. The CCN and extinction coefficient generally see sudden changes at identical time stamps after this adjustment. At the ground sites other than Svalbard, the nephelometer and PSAP instruments (see below) were downstream of a set of switched 1.0 μm and 10 μm impactors. This study uses the measurements behind the 10 μm impactor only. There is no aerosol size cut-off for the Svalbard data.

The light scattering and absorption of dried (RH~20%) particles were measured with TSI model 3563 nephelometers and Radiance Research particle soot absorption photometers (PSAP) at all locations. The sum of the scattering and absorption coefficient gives the extinction coefficient for dried particles. It is adjusted from two of the instrument wavelengths, 450 and 550 nm of the nephelometers and 470 and 530 nm of the PSAPs, to 500 nm assuming the linear relationship between the logarithm of coefficient and the logarithm of wavelength. The exception is the Svalbard single-wavelength (525 nm) PSAP, for which an absorption Angstrom exponent of unity is assumed. The extinction coefficient at 450 and 550 nm is also calculated, to derive the Angstrom exponent, α, again assuming the linear relationship on the logarithmic scales.

We estimate 5-10% as the uncertainty in the 500 nm dry extinction coefficient, σ. The uncertainty is smaller for finer particles (larger Angstrom exponent) due to smaller uncertainty in the nephelometer's angular truncation error (Anderson and Ogren, 1998). The uncertainty is set to 5% at minimum, because up to 7% differences have been reported between nephelometers (Heintzenberg et al., 2006). The ARM ground-based observations of extinction above 500 Mm^{-1} are screened out. We expect that this ceiling is seldom exceeded, with a possible exception of the dusty Niamey site in Niger.

CCN concentrations were measured using a Droplet Measurement Technologies streamwise thermal-gradient CCN counter (CCNC) (Lance et al., 2006; Lathem et al., 2013; Roberts and Nenes, 2005) at all locations. The CCNC consists of a cylindrical flow tube with wetted walls, on which a linear streamwise temperature gradient is applied. Owing to the greater diffusivity of water vapor than heat in air, a supersaturation is generated, which is highest at the center line of the flow tube. Sampled particles were exposed to the supersaturation along the vertical column. The supersaturation in the CCNC was corrected for the water vapor depletion due to high particle concentration during ARCTAS after Lathem et al. (2013). Activated particles were detected by an optical particle counter at the exit of the column. We estimate the uncertainty to be 10% of the best estimate plus 5 cm^{-3}. We exclude the CCN measurements at Southern Great Plains between May 20 and October 28, 2007 when the instrument temperature was not properly controlled.

This study also uses the aerosol size distributions measured with a scanning mobility particle sizer (SMPS) with a long differential mobility analyzer (TSI 3081 with custom electronics) in ARCTAS (McNaughton et al., 2011). The SMPS measured particles between 10 and 500 nm over a 60s period every 85s, for air volumes collected over 20s into a grab sampler. The grab chamber ensured that every point of each SMPS scan measures the particles from the same volume of air.

The CCN concentration observed during ARCTAS at the corrected instrument supersaturation between 0.3 and 0.5% was adjusted to a constant 0.4% using the aerosol size distribution measured with the SMPS. We first integrate the size distribution from the largest size bin until the concentration matches the measured CCN concentration (Lathem et al., 2013; Moore et al., 2011). The critical dry diameter determined this way is then adjusted from instrument supersaturation to 0.4% based on the Kohler theory to compute the CCN concentration at the

reference supersaturation. The adjusted CCN concentration is typically within 5% of the measured concentration. We did not make the adjustment for the data from other experiments.

The measured aerosol size distribution provides adequate counting accuracy and temporal resolution for the supersaturation adjustment. Matching or scaling with coincident condensation particle counter (CPC) measurements would exclude time periods when the aerosol number exceeded the CPC's upper detection limit, and otherwise has little influence on the adjustment of CCN concentration to a single supersaturation. The 1 Hz CPC counts indicate that plumes that lasted less than SMPS sample time or took place between the SMPS samples have negligible impact on the supersaturation adjustment. An assumption that 20% of the particles in each SMPS size bin are hydrophobic (i.e., external mixing), instead of internal mixing, also makes a negligible difference in the supersaturation adjustment according to our simulation.

Many recent studies have shown that the influence of aerosol composition on CCN activity can be efficiently represented by a single hygroscopicity parameter, κ, which simply expresses the affinity of a given aerosol particle for water (Petters and Kreidenweis, 2007). κ is near 0.1 for many organic species (Jimenez et al., 2009; Lathem et al., 2013) and 0.67 for ammonium sulfate (Petters and Kreidenweis, 2007). Derived κ is 0.03-0.16 for two thirds of the central Canada data, with a median of 0.08. This is plausible for the high organic content expected in the fresh biomass burning particles that we observed in central Canada. The arithmetic mean is 0.18, similar to the observations of biomass burning particles from the DC-8 aircraft in the same experiment (Lathem et al., 2013). The arithmetic mean is greater than the median and sensitive to a few data points with large values, as the histogram of the calculated κ values resembles a lognormal distribution rather than a normal one.

In ARCTAS, the 14-channel Ames Airborne Tracking Sunphotometer (AATS-14) measured direct solar beam transmission in narrow wavelength channels by using detectors in a tracking head mounted externally to the aircraft. It recorded 3s average data every 4s. The AATS-14 provides above-aircraft AOD with a small and well-characterized error (~0.01) at 13 wavelengths between 354 nm and 2139 nm. Shinozuka et al. (2011) describe data acquisition, screening, calibration, reduction and uncertainty analysis, as well as the vertical profiles, inter-comparison and fine-mode fraction of the AOD observed in ARCTAS. To compute the full-column AOD, below-aircraft contributions were estimated with coincident in situ observations under the assumption that the extinction coefficient for the ambient particles was

constant below the aircraft (at one kilometer or below). Specifically, the scattering coefficient was adjusted to the ambient humidity at the aircraft altitude, based on the f(RH) humidity response measured with a pair of nephelometers at ~20% and ~80% RH, before being added to the absorption coefficient and multiplied by the aircraft altitude. Note that the f(RH) adjustment imposed a negligible effect on our analysis because the ambient humidity was often below 50% over central Canada. The below-aircraft contributions thus calculated are 0-20% of the observed above-aircraft AOD in most cases. We assign half of the magnitude of this compensation, i.e., 0-10% of the above-aircraft AOD, as the best estimate of its uncertainty. This is combined with the 0.01 uncertainty in the above-aircraft AOD assuming these two components are independent of each other (calculated as the root of the sum of the squares), resulting in the uncertainty in the full-column AOD of 0.01-0.02 for most cases.

2.2 Resolution and Regression

McComiskey and Feingold (2012) say, "The ensuing effects of aggregation by averaging and loss of variance on common calculations of statistics […] are rarely discussed when inference is made from analyses of ACI at varying scales in the literature." Cantrell (2008) says, "While the literature is full of detailed analyses of procedures for fitting straight lines to values with uncertainties, a surprising number of scientists blindly use the standard least-squares method […] that assumes no uncertainties in the x values." Applying the appropriate regression method at the relevant resolution is important for the studies of CCN-extinction relationship where the analysis centers around regression. In this regard our study departs from previous ones in two ways.

First, this study minimizes data aggregation. Averaging data prior to regression generally improves correlation, but the results do not represent the variance of original data points. We do not average data over an entire experiment or CCN bins, because cloud microphysics occurs in scales much finer than hundreds of kilometers or weeks. We aggregate CCN and extinction data over 10-11s for the airborne data, 240-300s for the ground-based data. These time periods roughly correspond to one-kilometer horizontal distance for the typical P-3 ground speed near the surface (~120 m/s) and for the ground-based observations under the ~4 m/s winds. The aggregation is achieved by means of averaging, except for the data from the airborne nephelometers in which sample air resides for time periods comparable to 10s; we let a single scattering coefficient recorded in the middle of each time period represent it. The ARCTAS data are averaged over 11s instead of 10s with every 12th second discarded, to

encompass three AOD measurements instead of two. The data from the ARM ground sites are delivered as 60s averages. The first 60s CCN measurement after each supersaturation step is often influenced by the supersaturation instability and is removed. The rest are averaged over 240s. The Svalbard data are averaged over 300s.

Second, this study employs a bivariate regression method, with one over the estimated measurement uncertainty squared as weights for both x and y. When both x and y have uncertainties, the simple least-squares method underestimates the magnitude of the slope (see, for example, Cantrell (2008)). That leads to an underestimate of ∂logCCN/∂logAOD when x is logAOD and y is logCCN; an overestimate when, as in Andreae (2009) and Liu and Li (2014), x is logCCN and y is logAOD. Bivariate regression avoids this bias, as it gives the same slope regardless of the choice of variable for x and y by iteratively minimizing the sum of the squares of the diagonal distances (York et al., 2004). This feature forces the linear-correlation coefficient, R, to be near unity; we evaluate the goodness of the fit by two other measures. One is the variance of the slope estimated after Reed (1992) with the number of independent measurements determined with an autocorrelation analysis after Bretherton et al. (1999). The other is the root-mean-square (RMS) of the deviation of individual data points.

3 Results

3.1 The relationship of CCN to AOD and in situ dry extinction coefficient

Figure 1a compares the CCN concentration and AOD observed over central Canada during ARCTAS below one-kilometer altitude. Each grey circle represents the average over 11s in which our aircraft traveled a little over one-kilometer horizontal distance (see Section 2.2). The CCN concentration is adjusted to 0.4% supersaturation using the SMPS aerosol size distribution (Section 2.1). The 500 nm AOD presented here is measured with the upward-viewing AATS-14 and augmented for the below-aircraft contributions using coincident in situ aerosol extinction measurements. The resulting full-column AOD values are consistent with the AERONET ground-based observations within 0.02 for low-level fly-over events (Shinozuka et al., 2011).

The bivariate regression applied to $\log_{10}CCN_{SS=0.4\%}$ and $\log_{10}AOD_{500nm}$ yields a slope of 0.74±0.11, expressed as the best estimate ± the square root of the variance (one sigma). The RMS of the difference between the individual data points and fit is 0.35 on the $\log_{10}$ basis, which means that the fit estimates CCN concentrations within a factor of 2.3 ($10^{0.35}$, numbers

do not match due to rounding) of the observed value for about two thirds of the cases. A similar result is obtained from the standard least-squares regression (thin solid line): a slope of 0.71±0.19 and the deviation within a factor of 2.2. For the standard least-squares fit, the coefficient of determination (R^2) is 0.59. The similarity between the two regression results is expected for the relatively small measurement errors (see Section 2.1 and 2.2). The results appear insensitive to the choice of wavelength of the AOD: bivariate regression against the observed above-aircraft AOD spectra indicates that the RMS fitting error varies only by ±0.01 between 350 and 800 nm with little variation in the slope.

The deviations from the fit arise mainly from aerosol vertical profile and intensive properties. Of the other factors mentioned in Section 1, measurement errors are much smaller than a factor of 2.3. So is the impact of water uptake on AOD, owing to the low (mostly <50%) ambient RH and the low particle hygroscopicity in this environment. Aerosol horizontal-temporal variability is not an issue with the airborne observations where all instruments operated from a single platform at high temporal resolutions. If we minimize the impact of the vertical profile, we can focus on studying the impact of the intensive properties.

We remove the impact of the vertical profile by replacing the column integral AOD with the local extinction coefficient, in a manner similar to Shinozuka (2008) and Liu and Li (2014). Because the extinction coefficient is measured for dried particles, the impact of the humidity growth on light extinction is also removed. The slope remains similar, 0.75±0.05 (Figure 1b). The deviation is reduced from a factor of 2.3 to a factor of 1.7. As a reference, Figure 1b shows a line that goes through the geometric average of CCN (640 cm^{-3}) and σ (27 Mm^{-1}) with a slope of unity. It deviates most from the average of the CCN concentrations near the high and low ends of AOD.

The wide dynamic range of the ARCTAS data is advantageous for the regression analysis. If, for example, we remove extinction above 30 Mm^{-1}, both the square root of the variance of the estimated slope and the RMS fitting error amplify, from 0.05 and 1.7 to 0.17 and 2.0, respectively. x and y values that span narrow ranges should be avoided for the regression analysis.

The impact of the vertical profile is difficult to parameterize; so is that of the humidity response of extinction. Our strategy is to set these issues aside and examine the relationship between the coincident measurements of CCN concentration and extinction coefficient for

dried particles. The following subsection shows this relationship sorted by Angstrom exponent for ARCTAS and other experiments.

3.2 The CCN-extinction relationship for dried particles and its connection with Angstrom exponent

The slope and deviation are similar for other locations that cover a broad range of aerosol and meteorological environments. Figure 2 shows the subset of data from central Canada, Southern Great Plains, Cape Cod and Black Forest with an extinction Angstrom exponent between 1.5 and 1.7, and that from Ganges Valley, Graciosa Island, Svalbard and Niamey with an Angstrom exponent between 0.3 and 0.5. Data from the ground sites are averaged over 240-300s, which corresponds to about one-kilometer horizontal distance under typical wind speeds (Section 2.2). The slope is smaller than unity for all cases.

All CCN data shown here are measurements at 0.3-0.5% supersaturation. This range is wide enough to allow sufficient data for regression analysis. But it results in an isolated group of data points for a handful of cases, such as ~10% of the Black Forest data. This effect is evident despite the fact that data points up to one minute after each change in pre-set supersaturation are excluded. This is because the instrument supersaturation at the ARM ground sites, once recalculated for the actual instrument temperature, occasionally takes steps within the range, for example from just above 0.3% to just below 0.5%, rapidly changing the CCN concentration. The rate of this change varies with supersaturation and location. It is relatively high near 0.4% for Black Forest where the aerosol was highly variable with pollution from Stuttgart, organics from agriculture and nearby forest and heavy nitrate fertilization. Some of the isolated data points may be attributable to irregular instrument performance.

No adjustment to a single supersaturation value is made, except for the central Canada data. Adjustment is discouraged by the lack of supporting observations (e.g., size distribution) in a statistically significant volume. We refrain from scaling the CCN-extinction relationship with the supersaturation, because the observed relationship varies widely even over narrower ranges of supersaturation.

We applied the bivariate regression for other subsets of data. Figure 3a and Table 2 show regression results for the 0.2-wide Angstrom exponent bins where at least 100 data points exist with at least a factor of 1.5 variability, measured by the geometric standard deviation, in

both the CCN and extinction. For 85% of the bins, the best estimate of slope is between 0.5 and 1.0. The square root of the variance in the estimated slope is typically 0.03-0.2. The results are somewhat sensitive to the assumption on measurement uncertainty. The uncertainties assumed here, as detailed in Section 2.1, are 10% of the best estimate plus 5 cm^{-3} for the CCN, 5-10% for the extinction. Taken together, these considerations make us estimate that the expression 0.75±0.25 encompasses the one standard deviation range of the true values of the slope. The fitting error is between a factor of 1.5 and 2.0 for most cases (Figure 3b and Table 2). The exceptions are the data from Niamey, presumably due to the frequent presence of coarse dust particles that significantly contribute to extinction but are scarcely related to CCN number. Figure S1 in the supplementary materials shows that regression results are similar with 450 nm extinction instead of 500 nm. It also demonstrates that the standard least-squares method yields similar results whereas bisector and binned standard least-squares methods lead to significantly poorer fits.

Unlike the slope and deviation, the intercept shows a systematic trend with Angstrom exponent. To make the comparison among locations and Angstrom exponent bins easier, we recalculate the intercept for individual pairs of CCN and extinction for a fixed slope of 0.75, instead of using the bivariate regression results. Small dots in Figure 3c show the intercept for Graciosa Island as an example. The arithmetic mean of the intercept is indicated with bigger markers, for this location and others. The intercept increases with increasing Angstrom exponent. This is qualitatively consistent with the fact that smaller particles are generally more numerous for a given extinction. This effect is weaker for the data from pristine Svalbard (light green markers in Figure 3c), for unknown reasons. Since the linear fit is made on the $\log_{10}$-$\log_{10}$ coordinates, $10^{intercept}$ is an estimate of the geometric mean of the CCN concentrations at 1 Mm^{-1} dry extinction coefficient.

The mean intercept can be approximated as 0.3α+1.3 (dashed line in Figure 3c). Data from Niamey, Niger are excluded from this approximation for the presumed influence of dust, which is less prevalent than marine aerosols over the globe under warm and mixed-phase clouds. The approximation deviates widely from the Svalbard data over high Angstrom exponent values as well. This approximation completes the expression:

$$CCN_{SS\sim0.4\%}(cm^{-3})=10^{0.3\alpha+1.3}\sigma^{0.75} \qquad \text{(Eq. 1)}$$

where σ (Mm^{-1}) is the 500 nm extinction coefficient for dried particles and α, its Angstrom exponent. The estimated CCN concentration is within a factor of 2.0 of the individual

measurements, excluding Niamey (Figure 3d). The deviations tend to be greater, a factor of 10 for some, for observed CCN concentrations below 100 cm^{-3}. The deviation would be a factor of 2.7 without the use of Angstrom exponent.

The same analysis for other supersaturations (Figure S2, S3, S4 and S5 of the supplemental material) yields:

$$CCN_{SS\sim0.2\%}(cm^{-3})=10^{0.3\alpha+1.0}\sigma^{0.75} \quad \text{(Eq. 2)}$$

$$CCN_{SS\sim0.6\%}(cm^{-3})=10^{0.3\alpha+1.4}\sigma^{0.75} \quad \text{(Eq. 3)}$$

The exponent tends to slightly decrease with increasing supersaturation, as expected for the decreasing overlap between the optically important particles and CCN. But, because this tendency is dwarfed by the variability with location and Angstrom exponent, we have retained a slope of 0.75 for the parameterizations above. Note also that the parameterization for ~0.2% supersaturation is associated with a greater variability and fitting error (a factor of 3.0; Figure S3d) than for ~0.4% supersaturation. This is because a greater fraction of the observed CCN concentration is below 100 cm^{-3} and because variability among the locations is pronounced at this supersaturation.

4 Discussion

Based on the observed CCN-extinction relationship, we discuss underlying aerosol processes and satellite-based CCN estimates.

4.1 Indications of underlying aerosol processes

CCN concentration and dry extinction coefficient are each influenced by a host of aerosol processes, of production, transformation, mixing and removal, in air and clouds. The logCCN-vs-logσ relationship embodies the combined effect of the processes. Some drive the slope to less than unity. Some are responsible for the factor of 1.5-2.0 variability. Here we discuss such processes, especially those common for various locations and Angstrom exponent values. We present observed aerosol properties as circumstantial evidence for aerosol processes, noting that direct analysis with model simulations should be undertaken.

Recall that extinction is partly dependent on size and refractive index, not entirely on number. Two distributions that are similar in the Aitken mode concentrations may have a factor of ten difference in extinction, if they differ roughly tenfold in the accumulation mode. Spheres up

to 200 nm are more efficient at scattering with higher black carbon content (Figure 15.7 of Seinfeld and Pandis (2006)).

These phenomena are evident in the aerosol number size distribution observed in ARCTAS Canada. Figure 4a shows the distribution that is grouped by the concurrent 500 nm dry extinction coefficient and Angstrom exponent and averaged on the logarithmic scale. The accumulation mode varies with the extinction; the Aitken mode varies less.

To show the same data in a slightly different way, Figure 4b has the same grouped size distributions that are divided by the extinction and averaged (solid curves). Greater extinction is associated with proportionally fewer particles in the typical CCN sizes, one explanation for $\partial \log CCN/\partial \log \sigma < 1$. Two things might seem counter-intuitive. One is the de-emphasis of the Aitken mode with extinction up to 300 Mm^{-1}, given that the Angstrom exponent, which is commonly regarded as a size indicator, is restricted to 1.7-1.9 for this demonstration. The other is the lower peak height in the accumulation mode for extinction values beyond 300 Mm^{-1}, given that the distributions are normalized by the extinction. Simple Mie calculations applied to these distributions (dashed curves in Figure 4b) clarify that they are not odd. First, the particles up to ~100 nm have little influence on extinction. Variations in the Aitken mode have little influence on the Angstrom exponent in the detailed level, although the exponent does signal the CCN-extinction relationship to the extent shown in Figure 3c and reduces the typical deviation from a factor of 2.7 to 2.0. Second, the extinction distribution calculated for two refractive index values, 1.5-0.01i and 1.6-0.1i, demonstrates that a change in chemical composition can result in the same extinction with fewer accumulation-mode particles.

The de-emphasis of the Aitken mode may reflect aerosol growth processes. Coagulation, for example, decreases the number and increases the size. Condensation and in-cloud processing also make particles scatter more light while hardly increasing their number. Such ubiquitous processes may well be the primary reason for the similarity in the observed slope among the locations and Angstrom exponent bins.

The implied differences in refractive index, on the other hand, may reflect emissions and transformation unique to biomass burning particles. In ARCTAS, extinction values exceeding 300 Mm^{-1} were observed directly above flaming fires, with the SSA of 0.94±0.03. Values between 30-300 Mm^{-1} were observed around both flaming and smoldering fires, with an SSA of 0.97±0.02. The SSA difference might be a result of secondary aerosol production and

Deleted: single scattering albedo (

Deleted:)

oxidation, of the coatings on soot-containing particles among others, in addition to the diversity in combustion mechanisms.

Combustion mechanisms and post-emission physicochemical processes may be doubly effective in lowering the slope from unity, acting not only on refractive index but also on hygroscopicity. The critical dry diameter (see Section 2.1) tends to be greater, hence the CCN proportionally fewer, for greater extinction observed in the biomass burning particles (Figure 4a). The implied negative correlation between particle hygroscopicity and extinction might be attributable to the processes.

Besides the production and transformation, mixing and removal can conceivably influence the slope, although we do not have observational evidence. Dilution with clean air, for example, should work to bring the slope to unity, since optically effective particles and CCN are reduced by the same rate. So should the types of rain wash-out that scavenge particles regardless of their size and hygroscopicity. Such processes might explain slopes higher than 0.75 in some locations (Figure 3a, Table 2), though this might be caused by a few data points separate from the rest. Mixing, be it internal or external, of dust particles with hygroscopic particles can influence the slope, as indicated by the Niamey data (Figure 2 and 3, Table 2). Generally, fine-tuning of our parameterization for local meteorology and aerosol conditions should improve its accuracy.

Figure 4 helps explain not only the slope but also the variability in the CCN-extinction relationship. The shades in Figure 4b indicate the one geometric standard deviation range of the normalized size distributions, each of which corresponds to unit extinction and an Angstrom exponent near 1.8. As such, the shades, which encompass roughly ±70% of the geometric mean at most CCN sizes, represent the number of particles that can be added or removed without significantly influencing the extinction and its wavelength dependence. The variation in calculated critical diameter (horizontal bar in Figure 4a), by roughly ±40 nm, corresponds to a 40-60% variation in the CCN number and highlights its sensitivity to both size and hygroscopicity. The emissions and transformation of the biomass burning particles could be the main driver for the variability observed over central Canada, not just for the slope.

Deleted: the

Deleted: of CCN concentration

Of the two elements of the variability, the normalized size distribution is expected to depend partly on the choice of wavelength. But this dependence may be insignificant, because the particle sizes important for the number and the extinction are so far apart. The same

calculation for a wavelength of 350 nm instead of 500 nm would lower the extinction peak diameter from ~300 nm to ~210 nm, narrowing the difference from the number peak diameter (~100 nm) but not closing it. And the variability in the critical diameter would remain unchanged. This view makes it less surprising that the ARCTAS CCN-AOD relationship appears insensitive to the choice of wavelength of the AOD (Section 3.1). We need more extinction/AOD data that are spectrally wide and coincident with CCN measurements to study the impact of wavelength.

While our observation over central Canada is influenced by local biomass burning as the single dominant source, multiple emissions followed by mixing can also diversify the CCN-extinction relationship. The extinction coefficient at Graciosa Island with the Angstrom exponent between 0.3 and 0.5 should be dominated by coarse marine aerosols, setting aside occasional influences of dust. Fine pollution particles of continental origin may also be included in the extinction, but only to a degree that keeps the Angstrom exponent low. The CCN number, on the other hand, can be dominated by either pollution or marine aerosols. Specifically, continental outflow influences the site in the summer, whereas high wind speed increases marine aerosols in the winter (Clarke et al., 1997; Logan et al., 2014; Wood et al., 2014). The seasonal cycle thus contributes to the variability in CCN-extinction relationship (Figure 5): The average CCN concentration coincident with the extinction of 20±2 Mm^{-1}, for example, is 426 cm^{-3} in June, 245 cm^{-3} in December. Mixing in various time scales may also explain the high variability in the data from Black Forest and Cape Cod (Figure 2), sites that sample air masses with a number of different geographic origins. In fact, the location where data are collected appears to have a large impact on the variability (Figure 3b), in comparison with the Angstrom exponent which shows no obvious tendency with the RMS deviation. The deviation is not necessarily higher for smaller Angstrom exponent, as might be expected for the smaller overlap between optically important particles and CCN.

Any process that influences the particle hygroscopicity can contribute significantly to the variability around the dry CCN-extinction relationship. In general, knowledge of typical local aerosol size distribution and chemical composition helps constrain the impact of variation in hygroscopicity on the CCN concentration (Moore et al., 2012). While local observations and transport models can also help, these properties, especially the composition, are difficult to observe from satellite. Despite the negative correlation between the hygroscopicity and extinction, the CCN-extinction relationship in central Canada does not show a systematic

trend with SSA or f(RH=85%), optically observable indicators of particle composition. Such a trend, if present, must be obscured by the size and refractive index effects. Particle hygroscopicity is essentially ignored in the existing CCN parameterizations as well as in ours.

In another location the chemical composition is related to optical properties in a discernible manner. Shinozuka et al. (2009) find that the wavelength dependence of extinction was anti-correlated with the organic fraction of refractory mass of submicron particles (OMF) as $\alpha=-0.70\times OMF+2.0$ for Central Mexico's urban and industrial pollution. Shinozuka et al. (2009) and Russell et al. (2010) also show that absorption Angstrom exponent increased with the OMF, more rapidly for higher SSA, as expected for the interplay between soot, some organic species and dust. Such observations may assist remote sensing of aerosol chemical composition and CCN concentration in specific regions, making regional aerosol characterization an important element of improved satellite retrieval of CCN.

In principle, the discussion above would be less relevant if data were extensively aggregated. The aerosol physicochemical processes and transport phenomena would be less traceable in data averaged over, say, 1000 km or a year. Figure 6 shows the arithmetic mean and standard deviation of the CCN and dry extinction for each of the eight deployments with supersaturation between 0.3% and 0.5% and with no limit on Angstrom exponent. This figure lacks the spread of data points that is present in Figure 2 and Table 2. This figure hides the general trend that the CCN almost triples as the Angstrom exponent is increased from 0.5 to 2.0 in the finer resolution.

In practice, regression results do not change drastically upon aggregating the CCN and dry extinction. The slope through the deployment averages excluding Niamey is 0.90±0.19 with the bivariate regression (Section 2.2) when one over the standard deviation squared is used as weights for both x and y. This largely falls in the 0.75±0.25 range, though the one-sigma (the square root of the variance) value, 0.19, is greater than the values for the sorted fine-resolution data (Figure 2 and Table 2). Figure 6 also demonstrates that the standard least-squares method is sensitive to the choice of dependent and independent variables, to reiterate our remark in Section 2.2. $\partial\log CCN/\partial\log\sigma$ is 0.80 when x is $\log\sigma$ and y is logCCN, 0.94 when x is logCCN and y is $\log\sigma$.

The discussion above on aerosol processes, built on observed aerosol properties, remains to be verified with direct analysis. That probably requires model simulations. The slope between simulated CCN concentrations and dry extinction coefficient for a given location and

Angstrom exponent should be 0.75±0.25 to compare well with observations. Simulations without certain aerosol processes, coagulation and condensation for example, can reveal their impact on the CCN-extinction relationship and permit fine-tuning of their model representation.

Besides, co-variance of two aerosol properties should complement each of them as a model constraint. That is because taking the consistency between them should increase the chance that either property is estimated correctly. Think, as an example, a probabilistic evaluation of regional aerosol simulations where histograms are compared between simulations and observations separately for CCN concentration and dry extinction coefficient. The error in the estimate of each quantity may be obscured by its dynamic range and overlooked. This is less likely with the $CCN/\sigma^{0.75}$ ratio, because the CCN-σ relationship is tighter than is the dynamic range of either property. The relationship varies by a factor of 1.5-2.0 for most of the individual non-dusty locations and Angstrom exponent bins (Figure 3b, Table 2), whereas the dry extinction and CCN vary by a factor of 1.7-2.4 and 1.8-2.7, respectively (numbers given on the $\log_{10}$ basis in Table 2). Thus, the evaluation of the simulations would be more effective if the histograms of the ratio are considered in addition to those of each quantity.

4.2 Implications for satellite-based CCN estimates

The relationship of CCN to AOD, rather than to the dry extinction, is relevant to the satellite-based CCN estimates with passive sensors. The relationship is influenced considerably by the vertical profile of aerosols and their humidity growth. These strongly meteorology-dependent variables are difficult to parameterize and better left with transport models and direct observations to determine. Here we argue that, in general, these variables should not make logCCN-logAOD relationship steeper than the logCCN-logσ. We also consider how the variability in the CCN-AOD relationship is greater than that of the CCN-σ due to these variables as well as horizontal-temporal variability and measurement errors. We simulate CCN-AOD relationship for two scenarios, compare the results with the existing parameterizations and discuss implications for the study of ACI.

The relationship between boundary layer CCN concentration and column AOD in a given humidity environment is influenced by aerosol spatio-temporal distribution and intensive properties, as well as measurement errors (see Section 1). Our analysis of the central Canada data illustrates a way to isolate these influences from each other. The observed CCN-AOD

relationship in large part reflects the CCN-extinction relationship for dried particles within boundary layer air masses, as indicated by their resemblance in slope and a minor reduction in deviation (Section 3.1, compare Figure 1a and 1b). This data set is exceptionally suitable for demonstrating the resemblance, thanks primarily to the predominance of low-altitude aerosols, low RH and high organic content of the particles from local forest fires, as well as the wide dynamic ranges that make the regression robust.

For other environments the vertical profile and the humidity response of light extinction are harder to determine. But estimates can be made by a transport model (Chin et al., 2002; Heald et al., 2011; Koffi et al., 2012) or lidar observation with the aid of in situ dry measurements (Tesche et al., 2014; Ziemba et al., 2013). One can then reduce a satellite observation of AOD to the dry light extinction, for example by applying the following:

$$\sigma = (AOD - AOD_{str}) / H / f(RH) \qquad \text{(Eq. 4)}$$

where AOD_{str} is the stratospheric AOD and H, the aerosol layer thickness. f(RH) is the extinction coefficient of the ambient particles divided by that of dried particles, which is approximated by a scalar in this expression in spite of its altitude dependence. The extinction and its Angstrom exponent can then be inserted into Equation 1 to yield a CCN concentration estimate.

This strategy assumes that the CCN-extinction relationship found in our airborne (<1km altitude) and ground-based measurements holds for the cloud-base altitude. This assumption may or may not be valid. Ghan et al. (2006) find that the vertical profile of normalized dry extinction closely follows that of CCN concentration on most of the flights they examine, particularly within the lowest kilometer above the surface.

When estimating the CCN-AOD relationship, the uncertainties in the vertical profile and the humidity response needs to be combined with the factor of 2.0 error associated with our CCN-extinction parameterization. Uncertainties also arise from horizontal-temporal variability and measurement errors for the satellite-based estimates, though these additional factors are negligible for our airborne and ground-based data.

The presence of a dust layer aloft, for example, complicates the CCN-AOD relationship. The vertical profile depends on aerosol source and evolution as well as meteorological conditions, and may exert an uncertainty comparable with, or greater than, a factor of 2.0. The slope is also influenced and might be systematically decreased from 0.75±0.25, due to widening of the

relative dynamic range, as the dry extinction is replaced with AOD. A systematic increase in the slope is unlikely. It would imply a negative correlation between the aerosol layer depth and boundary-layer dry extinction coefficient. To be sure, a meteorology-aerosol connection is present in some regions. For example, the planetary boundary layer height generally increases and aerosol loading decreases away from the coast in the subtropical regions. But such a negative correlation is not known to exist systematically over the globe. Higher satellite resolution in vertical, horizontal and temporal dimensions, if achieved without significantly sacrificing AOD retrieval accuracy, will better constrain the relationship. Model estimates of aerosol layer thickness over wide horizontal and temporal extents will continue to be useful and might be improved with assimilated satellite data.

The response of light extinction to humidity changes is also difficult to ascertain, especially from remote sensing. Because the enhanced scattering due to water uptake by the particles can exceed a factor of 2.0 and varies widely in humid environment (Howell et al., 2006; Shinozuka et al., 2007; Tesche et al., 2014), its uncertainty might be comparable with or greater than a factor of 2.0, especially if the ambient humidity is unknown, high, or variable (Kapustin et al., 2006). In theory, the response of light extinction to humidity changes should be partly correlated with particle hygroscopicity, at least for aerosols whose chemical composition varies little with size. If such an association existed in humid environments, increases in light extinction would tend to be accompanied by lower critical dry diameter for activation and hence higher CCN concentrations. This would work to reduce the variability in the CCN per extinction and might help remote sensing of CCN concentration. However, such association is not evident in the central Canada data.

Like the vertical profile, the humidity response should randomly diversify the slope or, possibly, systematically decrease it. If the impact of hygroscopicity is greater on the AOD than on the CCN concentration, as is probably the case for all but hydrophobic particles in dry conditions, this effect may work to lower the slope when the extinction for dried particles is replaced with the ambient AOD for humid environment (not evident in the dry central Canada). A slope increase would imply higher f(RH) (i.e., higher RH, particle hygroscopicity or both) at lower dry extinction coefficient – possible but uncommon. Thus, while most of our observations (Section 3) refer to the in situ extinction of dried particles, it is logical to expect the relationship to the columnar ambient (not dried) AOD to have a slope smaller than unity as well.

The effects of horizontal-temporal variability are difficult to assess. The variability in the CCN concentration is partly a consequence of that in aerosol intensive properties such as size and hygroscopicity. This is accounted for in the factor of 2.0 error in our CCN-to-dry-extinction parameterization. Some of the horizontal-temporal variability in extensive properties is also accounted for, if the uncertainty in the estimate of vertical profile encompasses the horizontal-temporal variability of the vertical profile itself. The same is true for the humidity response of extinction. With the CCN-σ link, vertical profile and humidity response taken care of, the horizontal-temporal variability that remains to be accounted for is only of the AOD. More precisely, we should consider the AOD variability between the satellite and model grid boxes that is not included in the uncertainty estimate for the satellite AOD products, and enter this into the overall uncertainty in satellite-based CCN estimates. This way only the impact of the humidity response is double-counted.

The AOD horizontal-temporal variability within satellite grid boxes is negligible in comparison with other sources of uncertainty associated with AOD-based estimates of CCN. The AOD seldom varies by a few tens of percent within satellite grid cells (Shinozuka and Redemann, 2011) or within a time window in which the air travels tens of kilometers. This is small compared with the factor of 2.0 variability associated with the local dry CCN-extinction relationship. Note that the AOD presented in Shinozuka and Redemann (2011) is measured from a single aircraft and averaged over one-kilometer distance. The variability over one-kilometer distance must be generally smaller than that over 1x1 km^2 area, and is probably closer to that over 0.5x0.5 km^2 area (see Section 2.6 and Supplement of Shinozuka and Redemann (2011)). These statistics are meant to encompass two thirds of all cases. There are cases with higher variability. They include plumes from strong sources nearby and hydrophilic particles under high and variable humidity. Also, the variability is greater over longer distances, which matters if the CCN concentration for cloud pixels is to be estimated from AOD retrieved for clear-sky pixels hundreds of kilometers away.

Besides these aerosol properties, the satellite retrieval uncertainties can also pose a challenge to AOD-based estimates of the CCN concentration. For example, an AOD retrieval uncertainty of 30% translates into a 22% uncertainty in the CCN concentration because of the 0.75 exponent. An Angstrom exponent uncertainty of ±0.2 translates into a +15%/-13% uncertainty ($(10^{(\pm 0.2*0.3)}-1)\times 100\%$). If these two sources of uncertainties are independent of each other (which may not be correct), then the retrieval uncertainty alone makes the

estimated CCN uncertain by +26%/-25%. Satellite retrieval uncertainties may be greater, especially over land with passive sensors (Kahn et al., 2009; Levy et al., 2013; Levy et al., 2010) and for small AOD. An AOD error by 100% and an Angstrom exponent error by 0.5 result in a +80%/-74% uncertainty in the estimated CCN – comparable with our observed factor of 2.0.

We illustrate in Figure 7a how our CCN-σ parameterization can be translated into the CCN-AOD relationship for given scenarios. Values of the Angstrom exponent, layer depth, humidity response and AOD retrieval uncertainties are assumed separately for remote marine aerosols (0.2±0.2, 2±1 km, 3±1, ±0.03±0.05×AOD for AOD between 0.02 and 0.2; blue dashed curve) and polluted continental ones (2±0.2, 3±1.5 km, 2±0.5, ±0.05±0.15×AOD for AOD between 0.03 and 0.3; red dashed curve). The slight bend near AOD of 0.01 with both curves is caused by the assumed stratospheric AOD of 0.01 that is not converted to CCN. This treatment makes the CCN-AOD slope steeper for small AOD values that many satellite pixels, especially those in pristine marine conditions, observe. The uncertainties represented by shades were computed by means of Monte Carlo simulations for the factor of 2.0 variability of our parameterization and the assumed uncertainties indicated above. The overall uncertainties are a factor of ~3 for AOD_{500nm} <~0.1 and a little over a factor of 2 for the rest.

Experiment averages over hundreds of kilometres and months shown in Figure 1 and Table 2 of Andreae (2009) are marked in our Figure 7a with diamonds. Our simulations come fairly close to them. In this sense the two studies are mutually consistent. However, there are important differences. Our curves are less steep. Our results for multiple Angstrom exponent values do not form a single line. Our simulation here explicitly accounts for the vertical profile and the humidity effect on extinction. Data aggregation seems to influence regression in the logCCN-logAOD space, in a manner not possible in the logCCN-logσ space (Section 4.1, Figure 6): Indifference to the humidity effect and vertical profile seems to invite the logCCN-logAOD slope to appear greater than it actually is in finer scales within aerosol types. If so, this could mislead satellite-based estimates of ACI. Also, the use of standard least-squares regression may exacerbate the overestimate of the slope when uncertainties associated with both the CCN and AOD are large (see Section 2.2). The uncertainties in this context include the effect of the spatio-temporal gap between the two measurements.

AI can work well for fine particles. The dash-dot lines in Figure 7b show that with an adequate constant of proportionality (say, 3000), the 500 nm AOD multiplied by the

Angstrom exponent can predict the number concentration nearly as well as our measurement-based parameterization does.

However, two characteristics of this product deviate from the reality. First, AI decreases as rapidly as Angstrom exponent does. At $\alpha=0.2$, the AI-based CCN estimate is significantly lower than ours (blue curves in Figure 7b); at $\alpha<0$, AI is negative. Our parameterization, derived from log-log plots, always returns a positive CCN concentration as long as the extinction coefficient is positive.

Second, AI is proportional to the AOD with the Angstrom exponent kept unchanged. Nakajima et al. (2001) suggested raising the product to the power of 0.869, which subsequent studies neglected. Doing so would make it a better surrogate for CCN, closer to 0.75, the value we find through the direct observations. The parameterizations by Gassó and Hegg (2003) and Liu and Li (2014) also have a slope greater than ours (see Section 1).

The fact that the slope is smaller in our parameterization than any of the existing ones may have implications for satellite-based CCN estimates and ACI studies. The smaller slope, we expect, is translated into a smaller CCN variability, at least by a simplistic model where satellite AOD is directly converted to the CCN using such a parameterization. As a result, satellite-based estimates of radiative forcing through the interactions between aerosols and warm clouds may be lowered in magnitude. However, the differences arising from the choice of CCN-AOD parameterization may correspond to a considerably lower uncertainty in CDNC in the conditions where the cloud dynamics makes the response of CDNC to CCN sublinear (Morales Betancourt and Nenes, 2014).

5 Conclusions

Approximating the number concentration of CCN with satellite retrievals of AOD is common. The existing methods of this approximation have not been critically evaluated with observations at one-kilometer horizontal resolution. If satellite-based CCN estimates are to continue to complement purely model-based ones, what CCN-AOD relationship should we assume and how large is the associated uncertainty? This study has examined airborne and ground-based observations of aerosols to address these questions, and discussed underlying aerosol processes.

For a realistic estimate of the CCN concentration at the warm cloud base, we propose starting with the in situ extinction coefficient for dried particles. That is to take advantage of

increasingly available lidar observations and transport model products in combination with the columnar ambient AOD spectra from a passive satellite sensor. Determine the CCN concentration at 1 Mm^{-1} extinction by $10^{0.3\alpha+1.3}$ (cm^{-3}) where α is the Angstrom exponent, and multiply it by $\sigma^{0.75}$ for a given dry extinction coefficient σ (Mm^{-1}).

This approximation returns values within a factor of 2.0 of most of our direct measurements averaged over one-kilometer horizontal distance. This variability is, though large, finite. This means that a moderate level of connection exists between the CCN number and dry extinction, justifying the parameterization as an approximation. Further investigations on the impact of particle hygroscopicity and region-specific tailoring may improve the accuracy of our parameterization. The uncertainty in the CCN-AOD relationship arises not only from the uncertainty in the CCN-σ but also from the humidity response of light extinction, the vertical profile, the horizontal-temporal variability and the AOD measurement error. Depending on the quality of the estimate of these factors, the uncertainty can be closer to a factor of three.

The slope of the $\log_{10}$CCN-$\log_{10}\sigma$ relationship, 0.75±0.25, is smaller than any existing parameterization. Aerosol growth processes such as condensation, coagulation and in-cloud processing generally make particles scatter more light while hardly increasing their number. Other processes of production, transformation, mixing and removal may play a role too. Our observations and analysis should help to evaluate their representation by models.

It is logical to expect the logCCN-logAOD relationship for ambient (not dried) aerosols to have a slope smaller than unity as well. Exceptions may arise from extensive data aggregation over space, time or aerosol types and, possibly, from special meteorology-aerosol connections influencing the vertical profile or humidity growth. With the slope smaller than unity, a doubling of AOD is associated with less than a doubling of CCN. This marks a departure from existing CCN proxies such as AOD and AI, and can impact estimates of ACI.

Acknowledgements

We thank Teruyuki Nakajima, Kazuaki Kawamoto, Steve Howell, Steffen Freitag, Chris Terai, Allison McComiskey, Andreas Beyersdorf, Bruce Anderson, Phil Russell, John Livingston, Sam LeBlanc, Tom Ackerman, Masataka Shiobara, Rob Levy, Meloë Kacenelenbogen, Qian Tan, Kirk Knobelspiesse, Connor Flynn, Trish Quinn and the two anonymous reviewers for valuable input. Funding through NASA New (Early Career) Investigator Program (NNX12AO27G) is gratefully acknowledged. The Svalbard CCN

measurement was supported by the KOPRI project: NRF-2011-0021063. Aerosol observations at the Zeppelin station were supported by the Swedish EPA.

References

Anderson, T. L. and Ogren, J. A.: Determining aerosol radiative properties using the TSI 3563 integrating nephelometer, Aerosol Science and Technology, 29, 57-69, 1998.

Andreae, M. O.: Correlation between cloud condensation nuclei concentration and aerosol optical thickness in remote and polluted regions, Atmos. Chem. Phys., 9, 543-556, 2009.

Bellouin, N., Quaas, J., Morcrette, J. J., and Boucher, O.: Estimates of aerosol radiative forcing from the MACC re-analysis, Atmospheric Chemistry and Physics, 13, 2045-2062, 2013.

Boucher, O., D. Randall, P. Artaxo, C. Bretherton, G. Feingold, P. Forster, V.-M. Kerminen, Y. Kondo, H. Liao, U. Lohmann, P. Rasch, S.K. Satheesh, S. Sherwood, Stevens, B., and Zhang., X. Y.: Clouds and Aerosols. In: Climate Change 2013: The Physical Science Basis. Contribution of Working Group I to the Fifth Assessment Report of the Intergovernmental Panel on Climate Change [Stocker, T.F., D. Qin, G.-K. Plattner, M. Tignor, S.K. Allen, J. Boschung, A. Nauels, Y. Xia, V. Bex and P.M. Midgley (eds.)], Cambridge University Press, Cambridge, United Kingdom and New York, NY, USA., 2013. 2013.

Bréon, F.-M., Tanré, D., and Generoso, S.: Aerosol Effect on Cloud Droplet Size Monitored from Satellite, Science 10.1126/science.1066434, 295, 834-838, 2002.

Bretherton, C. S., Widmann, M., Dymnikov, V. P., Wallace, J. M., and Bladé, I.: The Effective Number of Spatial Degrees of Freedom of a Time-Varying Field, Journal of Climate, 12, 1990-2009, 1999.

Cantrell, C. A.: Technical Note: Review of methods for linear least-squares fitting of data and application to atmospheric chemistry problems, Atmos. Chem. Phys., 8, 5477-5487, 2008.

Chin, M., Ginoux, P., Kinne, S., Torres, O., Holben, B. N., Duncan, B. N., Martin, R. V., Logan, J. A., Higurashi, A., and Nakajima, T.: Tropospheric Aerosol Optical Thickness from the GOCART Model and Comparisons with Satellite and Sun Photometer Measurements, Journal of the Atmospheric Sciences, 59, 461-483, 2002.

Clarke, A. D., Uehara, T., and Porter, J. N.: Atmospheric nuclei and related aerosol fields over the Atlantic: Clean subsiding air and continental pollution during ASTEX, Journal of Geophysical Research, 102, 25281-25292, 1997.

Feingold, G. and Grund, C. J.: Feasibility of Using Multiwavelength Lidar Measurements to Measure Cloud Condensation Nuclei, Journal of Atmospheric and Oceanic Technology, 11, 1543-1558, 1994.

Gassó, S. and Hegg, D. A.: On the retrieval of columnar aerosol mass and CCN concentration by MODIS, Journal of Geophysical Research-Atmospheres, 108, 4010, doi:4010.1029/2002JD002382, 2003.

Ghan, S. J. and Collins, D. R.: Use of In Situ Data to Test a Raman Lidar–Based Cloud Condensation Nuclei Remote Sensing Method, Journal of Atmospheric and Oceanic Technology, 21, 387-394, 2004.

Ghan, S. J., Rissman, T. A., Elleman, R., Ferrare, R. A., Turner, D., Flynn, C., Wang, J., Ogren, J., Hudson, J., Jonsson, H. H., VanReken, T., Flagan, R. C., and Seinfeld, J. H.: Use of in situ cloud condensation nuclei, extinction, and aerosol size distribution measurements to test a method for retrieving cloud condensation nuclei profiles from surface measurements, Journal of Geophysical Research, 111, D05S10, doi:10.1029/2004JD005752, 2006.

Heald, C. L., Coe, H., Jimenez, J. L., Weber, R. J., Bahreini, R., Middlebrook, A. M., Russell, L. M., Jolleys, M., Fu, T. M., Allan, J. D., Bower, K. N., Capes, G., Crosier, J., Morgan, W. T., Robinson, N. H., Williams, P. I., Cubison, M. J., DeCarlo, P. F., and Dunlea, E. J.: Exploring the vertical profile of atmospheric organic aerosol: comparing 17 aircraft field campaigns with a global model, Atmospheric Chemistry and Physics, 11, 12673-12696, 2011.

Heintzenberg, J., Wiedensohler, A., Tuch, T. M., Covert, D. S., Sheridan, P., Ogren, J. A., Gras, J., Nessler, R., Kleefeld, C., Kalivitis, N., Aaltonen, V., Wilhelm, R. T., and Havlicek, M.: Intercomparisons and Aerosol Calibrations of 12 Commercial Integrating Nephelometers of Three Manufacturers, Journal of Atmospheric and Oceanic Technology, 23, 902-914, 2006.

Howell, S. G., Clarke, A. D., Shinozuka, Y., Kapustin, V., McNaughton, C. S., Huebert, B. J., Doherty, S. J., and Anderson, T. L.: Influence of relative humidity upon pollution and dust during ACE-Asia: Size distributions and implications for optical properties, Journal of Geophysical Research-Atmospheres, 111, D06205, doi:06210.01029/02004JD005759, 2006.

Huebert, B. J., Howell, S. G., Covert, D., Bertram, T., Clarke, A., Anderson, J. R., Lafleur, B. G., Seebaugh, W. R., Wilson, J. C., Gesler, D., Blomquist, B., and Fox, J.: PELTI: Measuring the Passing Efficiency of an Airborne Low Turbulence Aerosol Inlet, Aerosol Science and Technology, 38, 803-826, 2004.

Jacob, D. J., Crawford, J. H., Maring, H., Clarke, A. D., Dibb, J. E., Emmons, L. K., Ferrare, R. A., Hostetler, C. A., Russell, P. B., Singh, H. B., Thompson, A. M., Shaw, G. E., McCauley, E., Pederson, J. R., and Fisher, J. A.: The Arctic Research of the Composition of the Troposphere from Aircraft and Satellites (ARCTAS) mission: design, execution, and first results, Atmos. Chem. Phys., 10, 5191-5212, 2010.

Jefferson, A.: Empirical estimates of CCN from aerosol optical properties at four remote sites, Atmospheric Chemistry and Physics, 10, 6855-6861, 2010.

Jimenez, J. L., Canagaratna, M. R., Donahue, N. M., Prevot, A. S. H., Zhang, Q., Kroll, J. H., DeCarlo, P. F., Allan, J. D., Coe, H., Ng, N. L., Aiken, A. C., Docherty, K. S., Ulbrich, I. M., Grieshop, A. P., Robinson, A. L., Duplissy, J., Smith, J. D., Wilson, K. R., Lanz, V. A., Hueglin, C., Sun, Y. L., Tian, J., Laaksonen, A., Raatikainen, T., Rautiainen, J., Vaattovaara, P., Ehn, M., Kulmala, M., Tomlinson, J. M., Collins, D. R., Cubison, M. J., Dunlea, E. J., Huffman, J. A., Onasch, T. B., Alfarra, M. R., Williams, P. I., Bower, K., Kondo, Y., Schneider, J., Drewnick, F., Borrmann, S., Weimer, S., Demerjian, K., Salcedo, D., Cottrell, L., Griffin, R., Takami, A., Miyoshi, T., Hatakeyama, S., Shimono, A., Sun, J. Y., Zhang, Y. M., Dzepina, K., Kimmel, J. R., Sueper, D., Jayne, J. T., Herndon, S. C., Trimborn, A. M., Williams, L. R., Wood, E. C., Middlebrook, A. M., Kolb, C. E., Baltensperger, U., and Worsnop, D. R.: Evolution of Organic Aerosols in the Atmosphere, Science, 326, 1525-1529, 2009.

Kahn, R. A., Nelson, D. L., Garay, M. J., Levy, R. C., Bull, M. A., Diner, D. J., Martonchik, J. V., Paradise, S. R., Hansen, E. G., and Remer, L. A.: MISR Aerosol Product Attributes and Statistical Comparisons With MODIS, Geoscience and Remote Sensing, IEEE Transactions on, 47, 4095-4114, 2009.

Kapustin, V. N., Clarke, A. D., Shinozuka, Y., Howell, S., Brekhovskikh, V., Nakajima, T., and Higurashi, A.: On the determination of a cloud condensation nuclei from satellite: Challenges and possibilities, Journal of Geophysical Research-Atmospheres, 111, D04202, doi:04210.01029/02004JD005527, 2006.

Kaufman, Y. J., Koren, I., Remer, L. A., Rosenfeld, D., and Rudich, Y.: The effect of smoke, dust, and pollution aerosol on shallow cloud development over the Atlantic Ocean, Proceedings of the National Academy of Sciences, 10.1073/pnas.0505191102, 102, 11207-11212, 2005.

Koffi, B., Schulz, M., Bréon, F.-M., Griesfeller, J., Winker, D., Balkanski, Y., Bauer, S., Berntsen, T., Chin, M., Collins, W. D., Dentener, F., Diehl, T., Easter, R., Ghan, S., Ginoux, P., Gong, S., Horowitz, L. W., Iversen, T., Kirkevåg, A., Koch, D., Krol, M., Myhre, G., Stier, P., and Takemura, T.: Application of the CALIOP layer product to evaluate the vertical distribution of aerosols estimated by global models: AeroCom phase I results, Journal of Geophysical Research, 117, D10201, doi:10210.11029/12011JD016858, 2012.

Koren, I., Martins, J. V., Remer, L. A., and Afargan, H.: Smoke invigoration versus inhibition of clouds over the Amazon, Science, 321, 946-949, 2008.

Lance, S., Medina, J., Smith, J., and Nenes, A.: Mapping the Operation of the DMT Continuous Flow CCN Counter, Aerosol Science & Technology, 40, 242-254, 2006.

Lathem, T. L., Beyersdorf, A. J., Thornhill, K. L., Winstead, E. L., Cubison, M. J., Hecobian, A., Jimenez, J. L., Weber, R. J., Anderson, B. E., and Nenes, A.: Analysis of CCN activity of Arctic aerosol and Canadian biomass burning during summer 2008, Atmospheric Chemistry and Physics, 13, 2735-2756, 2013.

Levy, R. C., Mattoo, S., Munchak, L. A., Remer, L. A., Sayer, A. M., Patadia, F., and Hsu, N. C.: The Collection 6 MODIS aerosol products over land and ocean, Atmospheric Measurement Techniques, 6, 2989-3034, 2013.

Levy, R. C., Remer, L. A., Kleidman, R. G., Mattoo, S., Ichoku, C., Kahn, R., and Eck, T. F.: Global evaluation of the Collection 5 MODIS dark-target aerosol products over land, Atmospheric Chemistry and Physics, 10, 10399-10420, 2010.

Liu, J. and Li, Z.: Estimation of cloud condensation nuclei concentration from aerosol optical quantities: influential factors and uncertainties, Atmospheric Chemistry and Physics, 14, 471-483, 2014.

Liu, J., Zheng, Y., Li, Z., and Cribb, M.: Analysis of cloud condensation nuclei properties at a polluted site in southeastern China during the AMF-China Campaign, Journal of Geophysical Research, 116, 2011.

Logan, T., Xi, B., and Dong, X.: Aerosol properties and their influences on marine boundary layer cloud condensation nuclei at the ARM mobile facility over the Azores, Journal of Geophysical Research, 119, 4859-4872, 2014.

McComiskey, A. and Feingold, G.: The scale problem in quantifying aerosol indirect effects, Atmospheric Chemistry and Physics, 12, 1031-1049, 2012.

McNaughton, C. S., Clarke, A. D., Freitag, S., Kapustin, V. N., Kondo, Y., Moteki, N., Sahu, L., Takegawa, N., Schwarz, J. P., Spackman, J. R., Watts, L., Diskin, G., Podolske, J., Holloway, J. S., Wisthaler, A., Mikoviny, T., de Gouw, J., Warneke, C., Jimenez, J., Cubison, M., Howell, S. G., Middlebrook, A., Bahreini, R., Anderson, B. E., Winstead, E., Thornhill, K. L., Lack, D., Cozic, J., and Brock, C. A.: Absorbing aerosol in the troposphere of the Western Arctic during the 2008 ARCTAS/ARCPAC airborne field campaigns, Atmospheric Chemistry and Physics, 11, 7561-7582, 2011.

McNaughton, C. S., Clarke, A. D., Howell, S. G., Pinkerton, M., Anderson, B., Thornhill, L., Hudgins, C., Winstead, E., Dibb, J. E., Scheuer, E., and Maring, H.: Results from the DC-8

Inlet Characterization Experiment (DICE): Airborne Versus Surface Sampling of Mineral Dust and Sea Salt Aerosols Aerosol Science & Technology, 41, 136-159, 2007.

Moore, R. H., Bahreini, R., Brock, C. A., Froyd, K. D., Cozic, J., Holloway, J. S., Middlebrook, A. M., Murphy, D. M., and Nenes, A.: Hygroscopicity and composition of Alaskan Arctic CCN during April 2008, Atmos. Chem. Phys. Discuss., 11, 21789-21834, 2011.

Moore, R. H., Cerully, K., Bahreini, R., Brock, C. A., Middlebrook, A. M., and Nenes, A.: Hygroscopicity and composition of California CCN during summer 2010, Journal of Geophysical Research: Atmospheres, 117, D00V12, doi:10.1029/2011JD017352, 2012.

Morales Betancourt, R. and Nenes, A.: Understanding the contributions of aerosol properties and parameterization discrepancies to droplet number variability in a global climate model, Atmospheric Chemistry and Physics, 14, 4809-4826, 2014.

Müller, D., Hostetler, C. A., Ferrare, R. A., Burton, S. P., Chemyakin, E., Kolgotin, A., Hair, J. W., Cook, A. L., Harper, D. B., Rogers, R. R., Hare, R. W., Cleckner, C. S., Obland, M. D., Tomlinson, J., Berg, L. K., and Schmid, B.: Airborne Multiwavelength High Spectral Resolution Lidar (HSRL-2) observations during TCAP 2012: vertical profiles of optical and microphysical properties of a smoke/urban haze plume over the northeastern coast of the US, Atmospheric Measurement Techniques, 7, 3487-3496, 2014.

Nakajima, T., Higurashi, A., Kawamoto, K., and Penner, J. E.: A possible correlation between satellite-derived cloud and aerosol microphysical parameters, Geophysical Research Letters, 28, 1171-1174, 2001.

Penner, J. E., Xu, L., and Wang, M.: Satellite methods underestimate indirect climate forcing by aerosols, Proceedings of the National Academy of Sciences, 108, 13404-13408, 2011.

Penner, J. E., Zhou, C., and Xu, L.: Consistent estimates from satellites and models for the first aerosol indirect forcing, Geophys. Res. Lett., 39, L13810, doi:13810.11029/12012GL051870, 2012.

Petters, M. D. and Kreidenweis, S. M.: A single parameter representation of hygroscopic growth and cloud condensation nucleus activity, Atmospheric Chemistry and Physics, 7, 1961-1971, 2007.

Pringle, K. J., Tost, H., Pozzer, A., Pöschl, U., and Lelieveld, J.: Global distribution of the effective aerosol hygroscopicity parameter for CCN activation, Atmospheric Chemistry and Physics, 10, 5241-5255, 2010.

Pruppacher, H. R. and Klett, J. D.: Microphysics of Clouds and Precipitation, 1980. 1980.

Quaas, J., Boucher, O., Bellouin, N., and Kinne, S.: Satellite-based estimate of the direct and indirect aerosol climate forcing, Journal of Geophysical Research, 113, D05204, doi:05210.01029/02007JD008962, 2008.

Quaas, J., Boucher, O., and Bréon, F.-M.: Aerosol indirect effects in POLDER satellite data and the Laboratoire de Météorologie Dynamique-Zoom (LMDZ) general circulation model, Journal of Geophysical Research, 109, D08205, doi:08210.01029/02003JD004317, 2004.

Quaas, J., Ming, Y., Menon, S., Takemura, T., Wang, M., Penner, J. E., Gettelman, A., Lohmann, U., Bellouin, N., Boucher, O., Sayer, A. M., Thomas, G. E., McComiskey, A., Feingold, G., Hoose, C., KristjÃ¡nsson, J. E., Liu, X., Balkanski, Y., Donner, L. J., Ginoux, P. A., Stier, P., Grandey, B., Feichter, J., Sednev, I., Bauer, S. E., Koch, D., Grainger, R. G., Kirkevag, A., Iversen, T., Seland, Ã., Easter, R., Ghan, S. J., Rasch, P. J., Morrison, H.,

Lamarque, J. F., Iacono, M. J., Kinne, S., and Schulz, M.: Aerosol indirect effects - general circulation model intercomparison and evaluation with satellite data, Atmos. Chem. Phys., 9, 8697-8717, 2009.

Reed, B. C.: Linear least-squares fits with errors in both coordinates. II: Comments on parameter variances, Am. J. Phys., 60, 59–62, 1992.

Remer, L. A., Kaufman, Y. J., Mattoo, S., Martins, J. V., Ichoku, C., Levy, R. C., Kleidman, R. G., TanrÃ©, D., Chu, D. A., Li, R. R., Eck, T. F., Vermote, E., and Holben, B. N.: The MODIS Aerosol Algorithm, Products, and Validation, Journal of the Atmospheric Sciences, 62, 947-973, 2005.

Roberts, G. C. and Nenes, A.: A Continuous-Flow Streamwise Thermal-Gradient CCN Chamber for Atmospheric Measurements, Aerosol Science & Technology, 39, 206-221, 2005.

Russell, P. B., Bergstrom, R. W., Shinozuka, Y., Clarke, A. D., DeCarlo, P. F., Jimenez, J. L., Livingston, J. M., Redemann, J., Dubovik, O., and Strawa, A.: Absorption Angstrom Exponent in AERONET and related data as an indicator of aerosol composition, Atmos. Chem. Phys., 10, 1155-1169, 2010.

Sayer, A. M., Smirnov, A., Hsu, N. C., Munchak, L. A., and Holben, B. N.: Estimating marine aerosol particle volume and number from Maritime Aerosol Network data, Atmos. Chem. Phys., 12, 8889-8909, 2012.

Seinfeld, J. H. and Pandis, S. N.: Atmospheric Chemistry and Physics: From Air Pollution to Climate Change, 2nd Edition, Wiley, 2006. 2006.

Sekiguchi, M., T. Nakajima, K. Suzuki, K. Kawamoto, A. Higurashi, D. Rosenfeld, I. Sano, and Mukai, S.: A study of the direct and indirect effects of aerosols using global satellite data sets of aerosol and cloud parameters, Journal of Geophysical Research, 108, 4699, doi:4610.1029/2002JD003359, 2003.

Shinozuka, Y.: Relations between cloud condensation nuclei and aerosol optical properties relevant to remote sensing., PhD Thesis, Department of Oceanography, University of Hawaii at Manoa, 2008. 2008.

Shinozuka, Y., Clarke, A. D., DeCarlo, P. F., Jimenez, J. L., Dunlea, E. J., Roberts, G. C., Tomlinson, J. M., Collins, D. R., Howell, S. G., Kapustin, V. N., McNaughton, C. S., and Zhou, J.: Aerosol optical properties relevant to regional remote sensing of CCN activity and links to their organic mass fraction: airborne observations over Central Mexico and the US West Coast during MILAGRO/INTEX-B, Atmos. Chem. Phys., 9, 6727-6742, 2009.

Shinozuka, Y., Clarke, A. D., Howell, S. G., Kapustin, V. N., and Huebert, B. J.: Sea-salt vertical profiles over the Southern and tropical Pacific oceans: Microphysics, optical properties, spatial variability, and variations with wind speed, Journal of Geophysical Research, 109, D24201, doi:24210.21029/22004JD004975, 2004.

Shinozuka, Y., Clarke, A. D., Howell, S. G., Kapustin, V. N., McNaughton, C. S., Zhou, J., and Anderson, B. E.: Aircraft profiles of aerosol microphysics and optical properties over North America: Aerosol optical depth and its association with PM2.5 and water uptake, Journal of Geophysical Research, 112, D12S20, doi:10.1029/2006JD007918, 2007.

Shinozuka, Y. and Redemann, J.: Horizontal variability of aerosol optical depth observed during the ARCTAS airborne experiment, Atmos. Chem. Phys., 11, 8489-8495, 2011.

Shinozuka, Y., Redemann, J., Livingston, J. M., Russell, P. B., Clarke, A. D., Howell, S. G., Freitag, S., O'Neill, N. T., Reid, E. A., Johnson, R., Ramachandran, S., McNaughton, C. S.,

Kapustin, V. N., Brekhovskikh, V., Holben, B. N., and McArthur, L. J. B.: Airborne observation of aerosol optical depth during ARCTAS: vertical profiles, inter-comparison and fine-mode fraction, Atmos. Chem. Phys., 11, 3673-3688, 2011.

Tesche, M., Zieger, P., Rastak, N., Charlson, R. J., Glantz, P., Tunved, P., and Hansson, H. C.: Reconciling aerosol light extinction measurements from spaceborne lidar observations and in situ measurements in the Arctic, Atmospheric Chemistry and Physics, 14, 7869-7882, 2014.

Veselovskii, I., Kolgotin, A., Griaznov, V., Müller, D., Wandinger, U., and Whiteman, D. N.: Inversion with regularization for the retrieval of tropospheric aerosol parameters from multiwavelength lidar sounding, Applied Optics, 41, 3685-3699, 2002.

Waggoner, A. P., Weiss, R. E., Ahlquist, N. C., Covert, D. S., Will, S., and Charlson, R. J.: Optical characteristics of atmospheric aerosols, Atmospheric Environment (1967), 15, 1891-1909, 1981.

Wood, R., Wyant, M., Bretherton, C. S., Rémillard, J., Kollias, P., Fletcher, J., Stemmler, J., deSzoeke, S., Yuter, S., Miller, M., Mechem, D., Tselioudis, G., Chiu, C., Mann, J., O'Connor, E., Hogan, R., Dong, X., Miller, M., Ghate, V., Jefferson, A., Min, Q., Minnis, P., Palinkonda, R., Albrecht, B., Luke, E., Hannay, C., and Lin, Y.: Clouds, Aerosol, and Precipitation in the Marine Boundary Layer: An ARM Mobile Facility Deployment, Bulletin of the American Meteorological Society, doi: 10.1175/bams-d-13-00180.1, 2014. 140617093021002, 2014.

York, D., Evensen, N. M., Martínez, M. L., and Delgado, J. D. B.: Unified equations for the slope, intercept, and standard errors of the best straight line, American Journal of Physics, 72, 367-375, 2004.

Ziemba, L. D., Lee Thornhill, K., Ferrare, R., Barrick, J., Beyersdorf, A. J., Chen, G., Crumeyrolle, S. N., Hair, J., Hostetler, C., Hudgins, C., Obland, M., Rogers, R., Scarino, A. J., Winstead, E. L., and Anderson, B. E.: Airborne observations of aerosol extinction by in situ and remote-sensing techniques: Evaluation of particle hygroscopicity, Geophysical Research Letters, 40, 417-422, 2013.

Table 1. Data sets used in this study.

	Latitude	Longitude	Altitude (m)	Dates	Time Int. (s)	D (μm)$_{50\%}$
Central Canada (ARCTAS)	56°±6° N	109°±7° W	50-1000	2008/06-2008/07	11	>5
California, USA (DISCOVER-AQ)	37°±2° N	120°±2° W	50-1000	2013/01-2013/02	10	>5
Southern Great Plains, USA (ARM)	36° 36' 18" N	97° 29' 6" W	320	2006/09-2007/05, 2007/11-2008/07, 2008/09-2009/08, 2009/11-2011/03	240	10
Cape Cod, USA (ARM)	42° 1' 48" N	70° 2' 56" W	47	2012/07-2012/10, 2013/01-2013/05	240	10
Black Forest, Germany (ARM)	48° 32' 24" N	8° 23' 49" E	511	2007/04-2007/12	240	10
Ganges Valley, India (ARM)	29° 21' 34" N	79° 27' 29" E	1936	2011/06-2012/03	240	10
Graciosa Island, Azores (ARM)	39° 5' 28" N	28° 1' 45" W	15	2009/04-2009/12, 2010/07-2010/12	240	10
Svalbard	78° 54' 0'' N	11° 51' 60'' E	474	2009/01-2009/04, 2012/05-2012/12	300	Not Applied
Niamey, Niger (ARM)	13° 28' 39" N	2° 10' 28" E	205	2005/12-2006/05, 2006/08-2006/12	240	10

$D_{50\%}$ refers to the particle size for which the estimated passing efficiency is 50%.

Table 2. The results of bivariate regression analysis for 0.3-0.5% supersaturation.

Ang. Exp.	N	log10(Ext.)	log10(CCN)	Slope	Intercept	RMSe
Central Canada, 11s avg., ≤1 km alt.						
1.5-1.7	100	1.52±0.47	2.83±0.42	0.77±0.22	1.67±0.08	1.68
1.7-1.9	123	1.66±0.59	2.98±0.48	0.75±0.12	1.75±0.05	1.54
1.9-2.1	106	1.80±0.72	3.13±0.59	0.74±0.13	1.82±0.06	1.70
Southern Great Plains, USA, 240s avg.						
0.1-0.3	102	1.21±0.39	2.38±0.27	0.54±0.19	1.75±0.08	1.63
0.3-0.5	254	1.24±0.38	2.47±0.31	0.70±0.13	1.62±0.05	1.67
0.5-0.7	605	1.35±0.38	2.66±0.34	0.74±0.09	1.68±0.04	1.73
0.7-0.9	1473	1.42±0.37	2.78±0.31	0.61±0.05	1.93±0.03	1.71
0.9-1.1	3271	1.51±0.38	2.84±0.30	0.55±0.03	2.02±0.02	1.69
1.1-1.3	7141	1.55±0.33	2.90±0.28	0.58±0.03	2.02±0.01	1.66
1.3-1.5	11545	1.56±0.29	2.97±0.27	0.62±0.02	2.03±0.01	1.70
1.5-1.7	8260	1.53±0.28	3.05±0.29	0.77±0.03	1.89±0.01	1.69
1.7-1.9	2687	1.46±0.31	3.07±0.33	0.91±0.05	1.75±0.02	1.66
1.9-2.1	561	1.39±0.37	3.07±0.40	1.02±0.08	1.66±0.04	1.67
Cape Cod, USA, 240s avg.						
0.3-0.5	410	1.54±0.23	2.40±0.29	1.07±0.12	0.77±0.05	1.50
0.5-0.7	649	1.53±0.24	2.53±0.33	0.74±0.09	1.43±0.04	1.95
0.7-0.9	528	1.35±0.22	2.54±0.22	0.81±0.12	1.45±0.05	1.45
0.9-1.1	587	1.25±0.23	2.54±0.25	0.82±0.13	1.53±0.05	1.58
1.1-1.3	505	1.16±0.23	2.61±0.26	0.81±0.14	1.68±0.04	1.61
1.3-1.5	632	1.14±0.23	2.74±0.25	0.85±0.13	1.78±0.04	1.57
1.5-1.7	752	1.17±0.24	2.83±0.24	0.76±0.10	1.95±0.03	1.56
1.7-1.9	973	1.25±0.30	2.90±0.31	0.70±0.07	2.05±0.03	1.80
1.9-2.1	934	1.38±0.30	3.04±0.30	0.70±0.06	2.08±0.02	1.68
2.1-2.3	206	1.20±0.32	2.99±0.26	0.77±0.11	2.07±0.04	1.33
Black Forest, Germany, 240s avg.						
0.9-1.1	127	1.56±0.50	2.63±0.41	0.52±0.10	1.88±0.06	1.91
1.1-1.3	491	1.58±0.46	2.56±0.64	0.68±0.06	1.63±0.04	3.32
1.3-1.5	1522	1.58±0.36	2.79±0.42	0.72±0.04	1.70±0.03	2.06
1.5-1.7	2402	1.60±0.29	2.84±0.46	0.87±0.06	1.51±0.04	2.53
1.7-1.9	611	1.54±0.31	2.87±0.44	0.79±0.10	1.71±0.06	2.42
Ganges Valley, India, 240s avg.						
0.1-0.3	218	2.29±0.21	3.09±0.21	0.83±0.11	1.19±0.07	1.31
0.3-0.5	489	2.38±0.27	3.21±0.28	0.90±0.06	1.06±0.05	1.35
0.5-0.7	1738	2.37±0.25	3.23±0.26	0.96±0.04	0.96±0.03	1.34
0.7-0.9	3691	2.17±0.25	3.13±0.26	0.96±0.02	1.04±0.02	1.30
0.9-1.1	1994	1.88±0.28	2.93±0.33	1.02±0.03	1.03±0.02	1.42
1.1-1.3	778	1.50±0.23	2.55±0.40	1.33±0.09	0.60±0.04	1.74
Graciosa Island, Azores, 240s avg.						
-0.3--0.1	1496	1.56±0.24	2.27±0.24	0.90±0.03	0.89±0.03	1.50
-0.1-0.1	2031	1.51±0.26	2.46±0.25	0.81±0.02	1.24±0.03	1.52
0.1-0.3	2291	1.43±0.26	2.52±0.25	0.80±0.02	1.38±0.02	1.56
0.3-0.5	1462	1.33±0.26	2.60±0.26	0.87±0.02	1.44±0.02	1.46
0.5-0.7	933	1.25±0.28	2.63±0.27	0.81±0.03	1.62±0.02	1.45
0.7-0.9	597	1.22±0.26	2.69±0.25	0.79±0.04	1.73±0.04	1.52
0.9-1.1	296	1.21±0.31	2.74±0.30	0.76±0.05	1.83±0.05	1.60
Svalbard, 300s avg.						
-0.3--0.1	144	0.34±0.37	1.59±0.37	0.74±0.60	1.37±0.06	2.27
-0.1-0.1	141	0.47±0.35	1.68±0.35	0.89±0.73	1.27±0.08	2.21
0.1-0.3	207	0.49±0.38	1.71±0.34	0.73±0.26	1.39±0.04	1.97
0.3-0.5	215	0.66±0.55	1.87±0.45	0.63±0.16	1.51±0.03	1.99
0.5-0.7	321	0.56±0.37	1.79±0.35	0.76±0.23	1.40±0.03	1.88
0.7-0.9	407	0.61±0.33	1.84±0.30	0.76±0.23	1.40±0.03	1.78
0.9-1.1	545	0.63±0.37	1.90±0.29	0.80±0.19	1.39±0.03	1.94
1.1-1.3	618	0.68±0.31	1.94±0.32	0.92±0.19	1.33±0.03	1.73
1.3-1.5	733	0.70±0.32	1.99±0.31	0.87±0.17	1.39±0.03	1.70
1.5-1.7	630	0.71±0.33	2.02±0.30	0.71±0.15	1.54±0.02	1.65
1.7-1.9	408	0.65±0.36	2.00±0.34	0.67±0.20	1.59±0.03	1.76
1.9-2.1	284	0.56±0.32	1.95±0.33	0.85±0.32	1.49±0.04	1.82
2.1-2.3	180	0.46±0.28	1.99±0.33	1.44±0.90	1.23±0.09	2.53
2.3-2.5	118	0.30±0.30	1.86±0.38	1.42±0.98	1.37±0.07	2.22
Niamey, Niger, 240s avg.						
0.1-0.3	231	2.25±0.27	2.37±0.39	0.30±0.09	1.78±0.10	2.49
0.3-0.5	1557	2.20±0.29	2.46±0.50	0.45±0.04	1.61±0.05	3.19
0.5-0.7	1064	2.01±0.29	2.52±0.61	0.76±0.06	1.17±0.06	3.95
0.7-0.9	838	1.87±0.25	2.61±0.54	0.90±0.06	1.08±0.06	3.53
0.9-1.1	570	1.83±0.28	2.73±0.45	1.01±0.06	0.94±0.06	2.30
1.1-1.3	303	1.88±0.32	2.89±0.38	0.95±0.08	1.13±0.08	1.82
1.3-1.5	127	1.96±0.37	3.03±0.38	0.86±0.12	1.36±0.11	1.74

Ang. Exp. Is the Angstrom exponent of the extinction coefficient, N is the number of data points, the Ext. is the 500 nm extinction coefficient (Mm^{-1}) for dried particles, CCN is the

number of CCN concentration (cm^{-3}). RMSe given here is 10 raised to the root mean square of the fitting error; an RMSe of 2, for example, means that the deviation of individual data points is typically within a factor of 2 of the best estimate. The value after the ± symbol indicates the standard deviation or the square root of the variance.

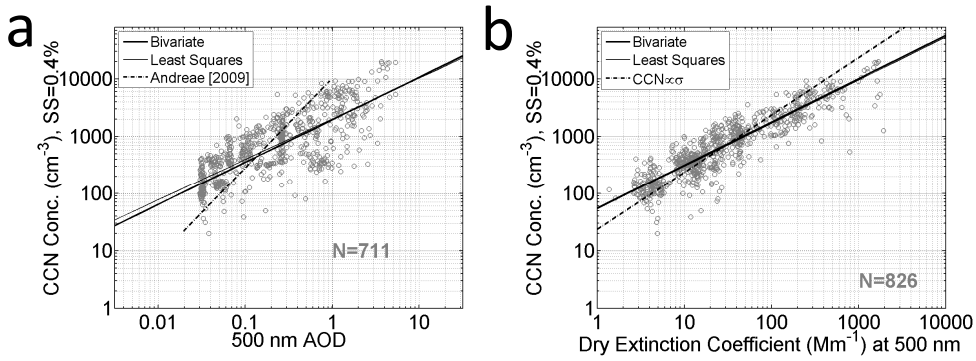

Figure 1. (a) CCN concentration and 500 nm AOD measured from the NASA P-3 aircraft over central Canada in summer 2008 during ARCTAS. Shown here is the subset of data from the lowest 1 km altitude with the CCN instrument supersaturation between 0.3% and 0.5%. The CCN concentration is adjusted to 0.4% supersaturation using the coincident measurements of aerosol size distribution and averaged over 11 seconds. The AOD from the airborne sunphotometer is augmented for the aerosols below the aircraft using simultaneous in situ measurements. The bivariate regression (thick solid line) on the 711 data points yields $CCN=1.9\times10^{3}AOD^{0.74\pm0.11}$, RMSe=2.3. The standard least-squares regression (thin solid line) yields $CCN=2.0\times10^{3}AOD^{0.71\pm0.19}$, R^2=0.59, RMSe=2.2. The expression from Andreae (2009), $AOD=0.0027CCN^{0.640}$, is also shown for reference (dash-dot line). (b) CCN concentration and 500 nm light extinction coefficient for dried particles, σ. The bivariate regression (thick solid line) on the 826 data points yields $CCN=55\sigma^{0.75\pm0.05}$, RMSe=1.7. The standard least-squares regression (thin solid line, nearly identical to the bivariate fit) yields $CCN=53\sigma^{0.75\pm0.09}$, R^2=0.82, RMSe=1.7. An expression that sets the CCN proportional to the extinction is also shown for reference (dash-dot line).

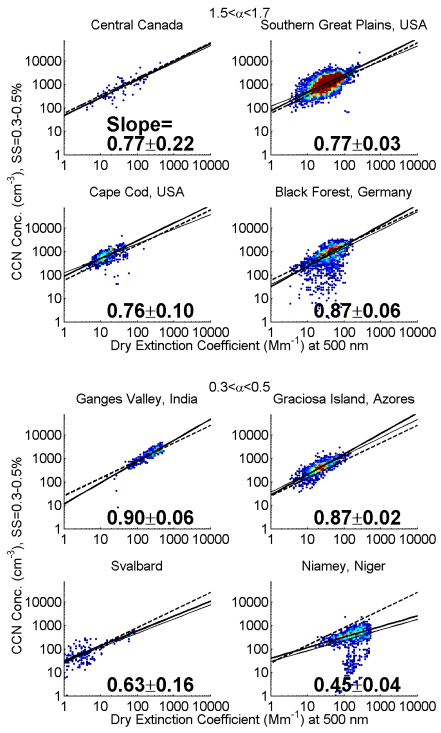

Figure 2. CCN and 500 nm extinction coefficient for dried particles measured over central Canada and at seven ground sites. The first four panels show the subset of data with the extinction Angstrom exponent between 1.7 and 1.9, and the last four, between 0.3 and 0.5. The number of data points is indicated by the color, blue for 1 and red for >20, for each square whose sides ($\Delta\log_{10}x$, $\Delta\log_{10}y$) are 0.05 long. The thick and thin solid lines represent the bivarite and standard least-squares linear regression, respectively. The dashed line represents our parameterization.

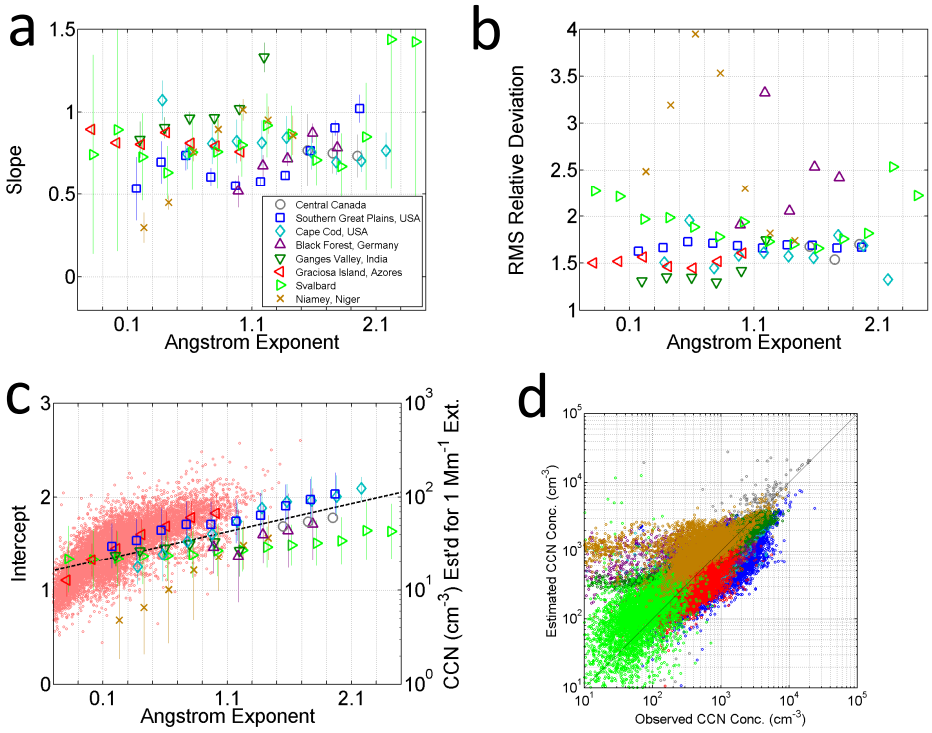

Figure 3. (a) The slope in $\log_{10}$CCN vs. $\log_{10}\sigma$ estimated by the bivariate linear regression for 0.2-wide Angstrom exponent bins. The square root of its variance is indicated by the vertical bar. (b) The RMS relative fitting error of the bivariate linear regression. (c) (dots) The intercept estimated for individual pairs of the CCN and extinction, calculated for a fixed slope of 0.75. This, plotted against the left axis, is identical to $\log_{10}$ of CCN concentration (cm^{-3}) estimated for 1 Mm^{-1} dry extinction coefficient at 500 nm (right axis). Only the Graciosa Island data are shown as an example. (bigger markers) The average and ±one standard deviation range of the intercept, for the Graciosa Island data (red) and other locations (other colors). The black dashed line represents our parameterization. (d) CCN concentration at 0.4% supersaturation estimated from our parameterization, compared with the observation at 0.3-0.5% supersaturation at the eight locations. See the legend in (a) for the locations. The RMS difference calculated for all but Niamey data is a factor of 2.0.

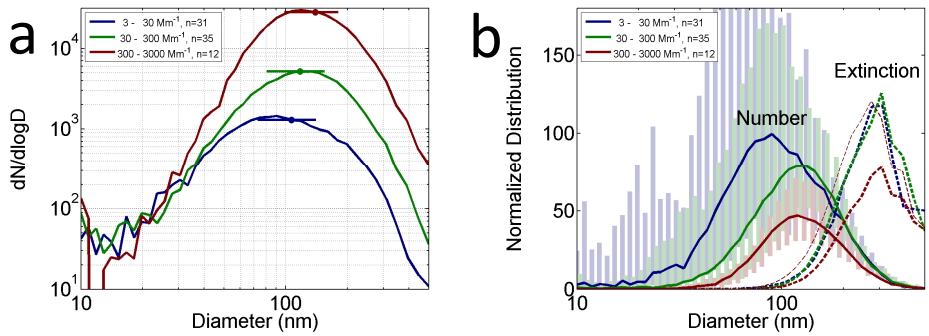

Figure 4. (a) The number size distribution ($dN/d\log_{10}D$ in the logarithmic scale) measured with an SMPS over central Canada at <1 km altitude during ARCTAS. The subset that coincides with an Angstrom exponent between 1.7 and 1.9 are shown, grouped by the 500 nm extinction coefficient for dried particles and averaged. The circle and horizontal bar indicates the mean and standard deviation of the dry critical diameter for 0.4% supersaturation. (b) The number and extinction size distributions divided by the extinction coefficient before being averaged. The unit is cm^{-3}/Mm^{-1} for the number (solid curves), non-dimensional times 100 for the extinction (dashed). The shade represents the one standard deviation range (encompassing the center 68%) of number distribution for each group. The extinction distribution is calculated for a refractive index of 1.5-0.01i (thick curves) and, for the 300-3000 Mm^{-1} extinction, 1.6-0.1i (thin). It does not sum to the observed extinction coefficient.

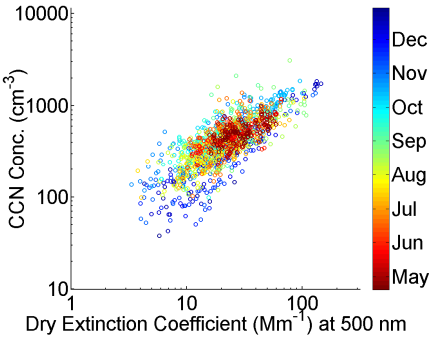

Figure 5. The Graciosa Island CCN-extinction relationship for the Angstrom exponent between 0.3-0.5 and supersaturation between 0.3-0.5%, color-coded with the time of the year in 2009 and 2010. No valid measurements are available between January and mid-April.

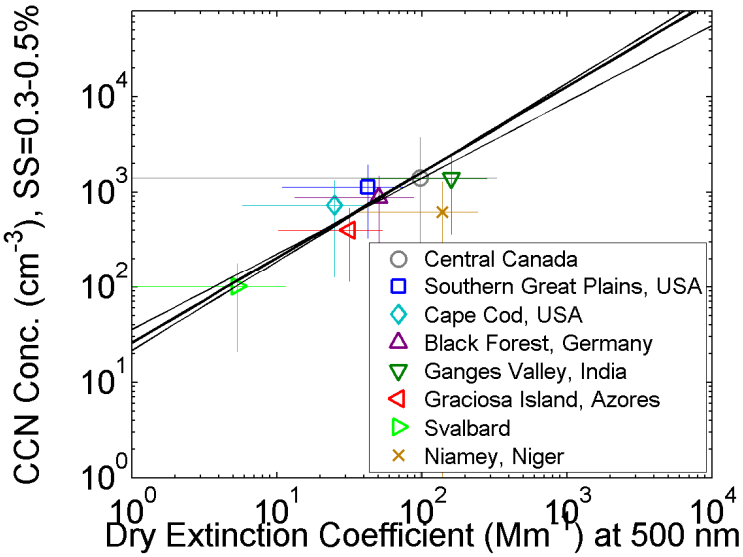

Figure 6. CCN and dry extinction averaged over each deployment. The bivariate regression (thick solid line) on the data points excluding Niamey, Niger yields $CCN=26\sigma^{0.90\pm0.19}$. The standard least-squares (thin solid lines) regression yields $CCN=35\sigma^{0.80}$ and, when $\log\sigma$ is chosen as dependent variable, $\sigma=3.8\times10^{-2}CCN^{1.07}$.

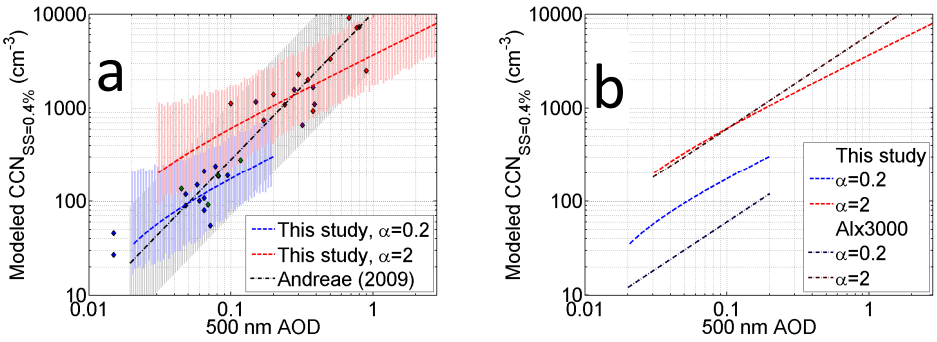

Figure 7. (a) CCN-AOD relationships simulated from the CCN-extinction parameterization for two scenarios (detailed in the text). The black dash-dot line represents the regression by Andreae (2009). It goes through averages over experiments in remote (blue and green diamonds) and polluted (purple and red) regions. (b) Same simulation results as (a). The uncertainty ranges are omitted for clarity. They are compared with the product of the 500 nm AOD, the Angstrom exponent and 3000.

The relationship between cloud condensation nuclei (CCN) concentration and light extinction of dried particles: indications of underlying aerosol processes and implications for satellite-based CCN estimates

Supplementary material

Table S1. The results of bivariate regression analysis for 0.1-0.3% supersaturation.

Ang. Exp.	N	log10(Ext.)	log10(CCN)	Slope	Intercept	RMSe
California, USA, 10s avg., \leq 1 km alt., 0.27% SS						
1.1-1.3	108	1.35±0.45	2.48±0.26	0.40±0.29	1.96±0.06	1.56
1.3-1.5	489	1.82±0.55	2.71±0.29	0.42±0.08	1.96±0.03	1.49
1.5-1.7	1017	1.90±0.40	2.84±0.28	0.59±0.07	1.73±0.03	1.45
1.7-1.9	1481	1.93±0.36	2.96±0.26	0.62±0.05	1.76±0.02	1.38
1.9-2.1	1859	1.87±0.29	3.02±0.19	0.55±0.05	1.99±0.02	1.28
2.1-2.3	1222	1.77±0.25	3.02±0.18	0.61±0.07	1.95±0.02	1.27
2.3-2.5	411	1.68±0.27	3.01±0.22	0.77±0.11	1.72±0.03	1.26
Southern Great Plains, USA, 240s avg.						
0.1-0.3	124	1.23±0.32	2.22±0.38	0.62±0.36	1.54±0.14	2.45
0.3-0.5	232	1.18±0.34	2.29±0.29	0.57±0.16	1.66±0.06	1.83
0.5-0.7	439	1.25±0.35	2.38±0.30	0.60±0.10	1.67±0.04	1.72
0.7-0.9	976	1.33±0.36	2.50±0.31	0.59±0.06	1.74±0.03	1.71
0.9-1.1	1927	1.42±0.36	2.59±0.31	0.59±0.04	1.78±0.02	1.68
1.1-1.3	3849	1.51±0.34	2.71±0.30	0.61±0.03	1.80±0.02	1.70
1.3-1.5	6472	1.55±0.31	2.78±0.31	0.67±0.03	1.76±0.02	1.76
1.5-1.7	5725	1.52±0.29	2.83±0.33	0.74±0.04	1.72±0.02	1.93
1.7-1.9	2814	1.48±0.30	2.87±0.32	0.74±0.05	1.79±0.02	1.81
1.9-2.1	887	1.41±0.34	2.88±0.36	0.89±0.08	1.63±0.04	1.77
2.1-2.3	200	1.24±0.31	2.81±0.34	1.04±0.17	1.52±0.07	1.61
Cape Cod, USA, 240s avg.						
0.3-0.5	242	1.51±0.20	2.13±0.28	1.13±0.24	0.46±0.10	1.63
0.5-0.7	408	1.53±0.23	2.28±0.36	0.93±0.14	0.90±0.06	2.09
0.7-0.9	257	1.35±0.22	2.23±0.29	0.95±0.21	0.98±0.08	1.74
0.9-1.1	282	1.22±0.22	2.21±0.29	0.94±0.19	1.11±0.06	1.70
1.1-1.3	304	1.15±0.22	2.25±0.30	1.03±0.20	1.09±0.06	1.71
1.3-1.5	329	1.14±0.22	2.33±0.29	0.84±0.21	1.41±0.07	1.85
1.5-1.7	382	1.14±0.23	2.42±0.28	0.75±0.19	1.59±0.06	1.85
1.7-1.9	543	1.25±0.30	2.52±0.37	0.78±0.11	1.59±0.04	2.05
1.9-2.1	381	1.33±0.34	2.57±0.48	0.75±0.11	1.66±0.04	2.7
Black Forest, Germany, 240s avg.						
0.9-1.1	349	1.58±0.50	1.75±0.61	0.34±0.10	1.53±0.07	3.96
1.1-1.3	1223	1.69±0.44	1.87±0.60	0.54±0.07	1.22±0.05	3.53
1.3-1.5	3763	1.64±0.35	1.98±0.56	0.74±0.05	0.98±0.03	3.28
1.5-1.7	5279	1.62±0.28	2.04±0.56	1.05±0.06	0.55±0.04	3.42
1.7-1.9	1422	1.55±0.30	1.98±0.59	0.99±0.11	0.68±0.07	3.73
Ganges Valley, India, 240s avg.						
0.1-0.3	245	2.26±0.21	2.41±0.49	2.45±0.58	-3.07±0.40	2.79
0.3-0.5	549	2.38±0.25	2.59±0.46	1.54±0.23	-1.02±0.17	2.37
0.5-0.7	2233	2.38±0.24	2.70±0.39	1.34±0.10	-0.47±0.08	2.09
0.7-0.9	4524	2.17±0.26	2.56±0.41	0.92±0.06	0.64±0.04	2.23
0.9-1.1	2396	1.90±0.28	2.31±0.45	0.73±0.07	1.04±0.04	2.59
1.1-1.3	858	1.50±0.24	1.89±0.53	1.14±0.15	0.35±0.07	2.91
Graciosa Island, Azores, 240s avg.						
-0.5--0.3	202	1.42±0.29	1.66±0.26	0.54±0.08	0.96±0.09	1.65
-0.3--0.1	2913	1.56±0.24	1.93±0.26	0.92±0.02	0.52±0.03	1.60
-0.1-0.1	4117	1.51±0.26	2.11±0.28	0.86±0.02	0.85±0.02	1.62
0.1-0.3	4438	1.43±0.26	2.19±0.28	0.78±0.02	1.10±0.02	1.65
0.3-0.5	2865	1.33±0.26	2.25±0.28	0.83±0.02	1.18±0.02	1.62
0.5-0.7	1819	1.27±0.27	2.29±0.29	0.78±0.02	1.33±0.02	1.61
0.7-0.9	1127	1.22±0.27	2.31±0.31	0.88±0.03	1.26±0.03	1.69
0.9-1.1	625	1.22±0.30	2.38±0.33	0.87±0.04	1.36±0.04	1.68
1.1-1.3	186	1.14±0.31	2.33±0.34	0.72±0.08	1.57±0.07	1.91
Svalbard, 300s avg.						
-0.3--0.1	142	0.45±0.34	1.50±0.36	0.51±0.39	1.38±0.04	2.21
-0.1-0.1	212	0.45±0.32	1.54±0.33	0.50±0.28	1.40±0.03	2.01
0.1-0.3	233	0.44±0.36	1.53±0.45	0.67±0.24	1.32±0.03	2.42
0.3-0.5	362	0.68±0.55	1.73±0.38	0.51±0.11	1.46±0.02	1.85
0.5-0.7	392	0.57±0.35	1.71±0.40	0.65±0.16	1.42±0.02	2.14
0.7-0.9	451	0.58±0.32	1.76±0.35	0.73±0.17	1.38±0.02	1.93
0.9-1.1	746	0.49±0.44	1.92±0.35	-0.21±0.11	2.17±0.01	2.45
1.1-1.3	807	0.67±0.32	1.89±0.34	0.86±0.12	1.33±0.02	1.74
1.3-1.5	872	0.72±0.32	1.96±0.34	0.90±0.12	1.33±0.02	1.78
1.5-1.7	829	0.76±0.31	2.00±0.34	0.87±0.11	1.36±0.02	1.67
1.7-1.9	596	0.70±0.34	1.96±0.35	0.79±0.13	1.44±0.02	1.71
1.9-2.1	360	0.61±0.35	1.88±0.36	0.68±0.20	1.53±0.03	2.13
2.1-2.3	185	0.42±0.33	1.80±0.40	0.89±0.37	1.46±0.04	2.00
2.3-2.5	118	0.37±0.26	1.78±0.31	1.28±0.91	1.28±0.07	1.77
Niamey, Niger, 240s avg.						
0.1-0.3	174	2.34±0.27	1.70±0.39	0.60±0.21	0.49±0.24	2.54
0.3-0.5	1271	2.21±0.27	1.62±0.52	0.56±0.07	0.72±0.08	4.08
0.5-0.7	1068	1.92±0.27	1.62±0.62	0.42±0.07	1.24±0.07	5.57
0.7-0.9	1169	1.77±0.22	1.82±0.55	0.38±0.08	1.42±0.07	4.22
0.9-1.1	952	1.75±0.22	1.95±0.46	0.47±0.09	1.32±0.08	3.16
1.1-1.3	620	1.75±0.26	1.94±0.49	0.47±0.10	1.32±0.09	3.30
1.3-1.5	252	1.82±0.31	2.05±0.47	0.39±0.15	1.55±0.13	3.23
1.5-1.7	138	1.85±0.33	2.14±0.49	0.75±0.21	0.90±0.20	2.86

Ang. Exp. Is the Angstrom exponent of the extinction coefficient, N is the number of data points, the Ext. is the 500 nm extinction coefficient (Mm^{-1}) for dried particles, CCN is the number of CCN concentration (cm^{-3}). RMSe given here is 10 raised to the root mean square of the fitting error; an RMSe of 2, for example, means that the deviation of individual data points is typically within a factor of 2 of the best estimate. The values after the ± symbol indicates the standard deviation or the square root of the variance.

Table S2. The results of bivariate regression analysis for 0.5-0.7% supersaturation.

Ang. Exp.	N	log10(Ext.)	log10(CCN)	Slope	Intercept	RMSe
Southern Great Plains, USA, 240s avg.						
0.5-0.7	209	1.34±0.37	2.81±0.35	0.65±0.16	1.98±0.07	2.00
0.7-0.9	471	1.43±0.39	2.90±0.37	0.56±0.11	2.14±0.05	2.10
0.9-1.1	1126	1.49±0.36	2.96±0.33	0.54±0.07	2.18±0.03	1.89
1.1-1.3	2597	1.53±0.33	3.01±0.32	0.53±0.05	2.23±0.02	1.89
1.3-1.5	4391	1.55±0.31	3.10±0.28	0.54±0.04	2.28±0.02	1.75
1.5-1.7	3457	1.52±0.29	3.16±0.30	0.72±0.05	2.07±0.02	1.76
1.7-1.9	1646	1.49±0.31	3.16±0.33	0.88±0.06	1.85±0.03	1.74
1.9-2.1	381	1.40±0.36	3.15±0.39	1.02±0.12	1.72±0.06	1.77
Cape Cod, USA, 240s avg.						
0.3-0.5	215	1.69±0.23	2.55±0.26	0.93±0.18	0.98±0.08	1.46
0.5-0.7	293	1.59±0.20	2.64±0.44	0.82±0.21	1.41±0.09	2.68
0.7-0.9	310	1.39±0.21	2.71±0.21	0.64±0.20	1.84±0.07	1.53
0.9-1.1	331	1.30±0.25	2.75±0.25	0.75±0.19	1.78±0.07	1.64
1.1-1.3	450	1.24±0.25	2.83±0.25	0.68±0.13	2.00±0.04	1.63
1.3-1.5	530	1.21±0.27	2.91±0.23	0.60±0.11	2.19±0.04	1.54
1.5-1.7	509	1.18±0.29	2.95±0.23	0.56±0.11	2.30±0.04	1.54
1.7-1.9	598	1.35±0.34	3.08±0.26	0.51±0.08	2.41±0.03	1.60
1.9-2.1	643	1.40±0.30	3.15±0.31	0.55±0.08	2.40±0.03	1.86
2.1-2.3	119	1.26±0.28	3.16±0.23	0.70±0.20	2.29±0.06	1.39
Black Forest, Germany, 240s avg.						
0.9-1.1	104	1.60±0.49	2.91±0.34	0.58±0.09	1.99±0.05	1.51
1.1-1.3	393	1.63±0.47	2.92±0.36	0.60±0.05	1.96±0.03	1.65
1.3-1.5	1319	1.61±0.37	3.03±0.30	0.63±0.04	2.03±0.02	1.56
1.5-1.7	1929	1.61±0.28	3.13±0.30	0.71±0.04	2.00±0.02	1.69
1.7-1.9	477	1.55±0.30	3.14±0.33	0.73±0.06	2.02±0.04	1.76
Ganges Valley, India, 240s avg.						
0.3-0.5	170	2.37±0.26	3.31±0.28	0.94±0.13	1.08±0.09	1.37
0.5-0.7	669	2.38±0.23	3.34±0.26	1.01±0.09	0.93±0.06	1.42
0.7-0.9	1423	2.16±0.25	3.24±0.26	0.92±0.04	1.25±0.03	1.34
0.9-1.1	791	1.90±0.29	3.11±0.32	0.99±0.06	1.25±0.03	1.40
1.1-1.3	280	1.53±0.25	2.81±0.37	1.26±0.16	0.90±0.08	1.63
1.3-1.5	134	1.22±0.18	2.45±0.35	1.62±0.36	0.50±0.13	1.73
Graciosa Island, Azores, 240s avg.						
-0.5--0.3	118	1.38±0.30	2.07±0.28	0.87±0.13	0.89±0.13	1.76
-0.3--0.1	1488	1.57±0.23	2.36±0.24	0.97±0.04	0.85±0.04	1.61
-0.1-0.1	2038	1.51±0.26	2.56±0.26	0.84±0.03	1.30±0.03	1.62
0.1-0.3	2267	1.43±0.26	2.61±0.26	0.83±0.03	1.43±0.03	1.65
0.3-0.5	1446	1.33±0.26	2.69±0.26	0.89±0.03	1.52±0.03	1.51
0.5-0.7	904	1.26±0.27	2.74±0.24	0.73±0.03	1.82±0.03	1.45
0.7-0.9	581	1.22±0.26	2.76±0.27	0.85±0.05	1.74±0.04	1.58
0.9-1.1	318	1.20±0.32	2.81±0.32	0.76±0.06	1.91±0.05	1.69
Svalbard, 300s avg.						
-0.1-0.1	129	0.52±0.37	1.75±0.32	0.71±0.70	1.40±0.08	2.09
0.1-0.3	166	0.42±0.32	1.77±0.40	1.21±0.78	1.23±0.08	2.81
0.3-0.5	245	0.67±0.52	1.92±0.43	0.66±0.18	1.53±0.03	1.97
0.5-0.7	293	0.57±0.33	1.89±0.33	0.97±0.43	1.32±0.06	2.26
0.7-0.9	435	0.62±0.33	1.87±0.31	0.79±0.25	1.39±0.04	1.86
0.9-1.1	522	0.63±0.34	1.91±0.33	0.93±0.24	1.32±0.04	1.99
1.1-1.3	614	0.71±0.31	1.99±0.31	0.96±0.21	1.30±0.03	1.81
1.3-1.5	711	0.72±0.30	2.03±0.30	0.93±0.21	1.35±0.03	1.81
1.5-1.7	615	0.72±0.30	2.05±0.28	0.89±0.21	1.40±0.03	1.72
1.7-1.9	450	0.67±0.35	2.03±0.31	0.74±0.22	1.55±0.03	1.77
1.9-2.1	280	0.57±0.32	2.01±0.36	0.91±0.44	1.49±0.06	2.14
2.1-2.3	172	0.40±0.32	1.92±0.38	1.37±0.83	1.27±0.09	2.56
Niamey, Niger, 240s avg.						
0.1-0.3	238	2.26±0.27	2.51±0.34	0.49±0.10	1.44±0.12	2.13
0.3-0.5	1479	2.19±0.30	2.65±0.44	0.45±0.04	1.73±0.04	2.64
0.5-0.7	924	2.02±0.30	2.78±0.45	0.74±0.05	1.35±0.05	2.51
0.7-0.9	784	1.85±0.26	2.84±0.33	0.98±0.05	1.05±0.05	1.80
0.9-1.1	544	1.82±0.28	2.95±0.33	0.98±0.05	1.17±0.04	1.60
1.1-1.3	300	1.84±0.30	3.05±0.32	0.99±0.06	1.24±0.05	1.43
1.3-1.5	134	1.92±0.37	3.21±0.34	0.87±0.07	1.55±0.07	1.41

Ang. Exp. Is the Angstrom exponent of the extinction coefficient, N is the number of data points, the Ext. is the 500 nm extinction coefficient (Mm^{-1}) for dried particles, CCN is the number of CCN concentration (cm^{-3}). RMSe given here is 10 raised to the root mean square of the fitting error; an RMSe of 2, for example, means that the deviation of individual data

points is typically within a factor of 2 of the best estimate. The values after the ± symbol indicates the standard deviation or the square root of the variance.

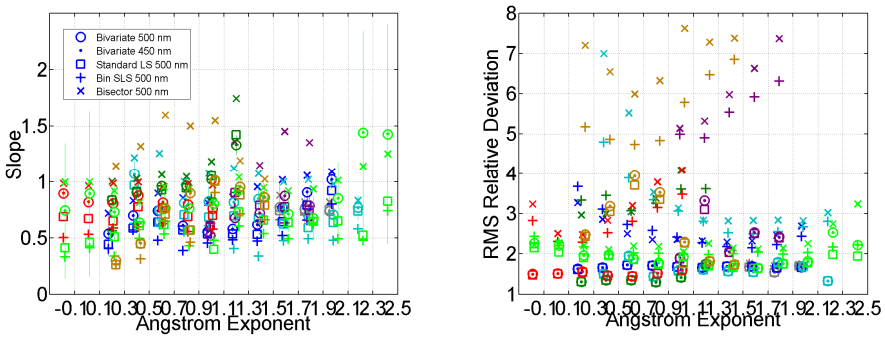

Figure S1. Results of additional regression analysis. The color corresponds to the locations indicated in Figure 3a. The dot is for the 450 nm extinction coefficient; all others are for 500 nm. The square is for the standard least-squares method, the plus for the same method applied after the individual data points are averaged over 0.5-wide $\log_{10}\sigma$ bins, and the cross for the bisector method. The two bivariate markers and the standard least-squares overlap between each other in several cases, especially for the RMS relative deviation.

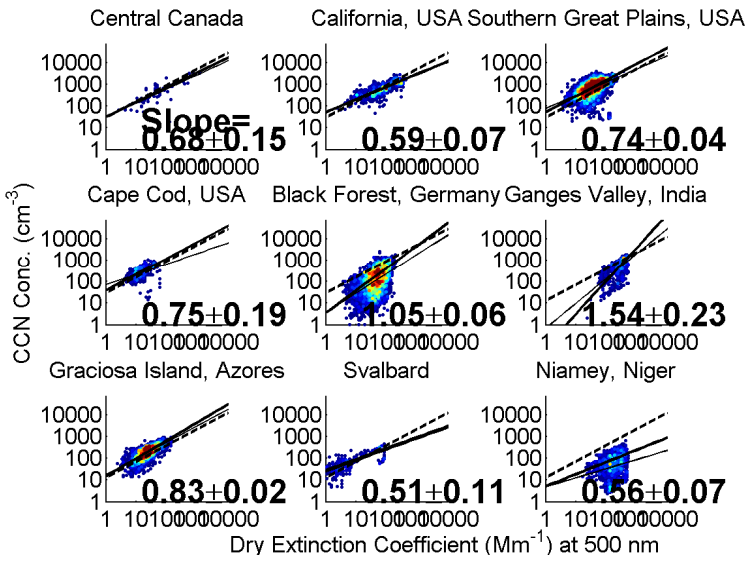

Figure S2. Same as Figure 2 but for supersaturation of 0.1-0.3% instead of 0.3-0.5%. This includes data from DISCOVER-AQ California for Angstrom exponent between 1.7 and 1.9.

1

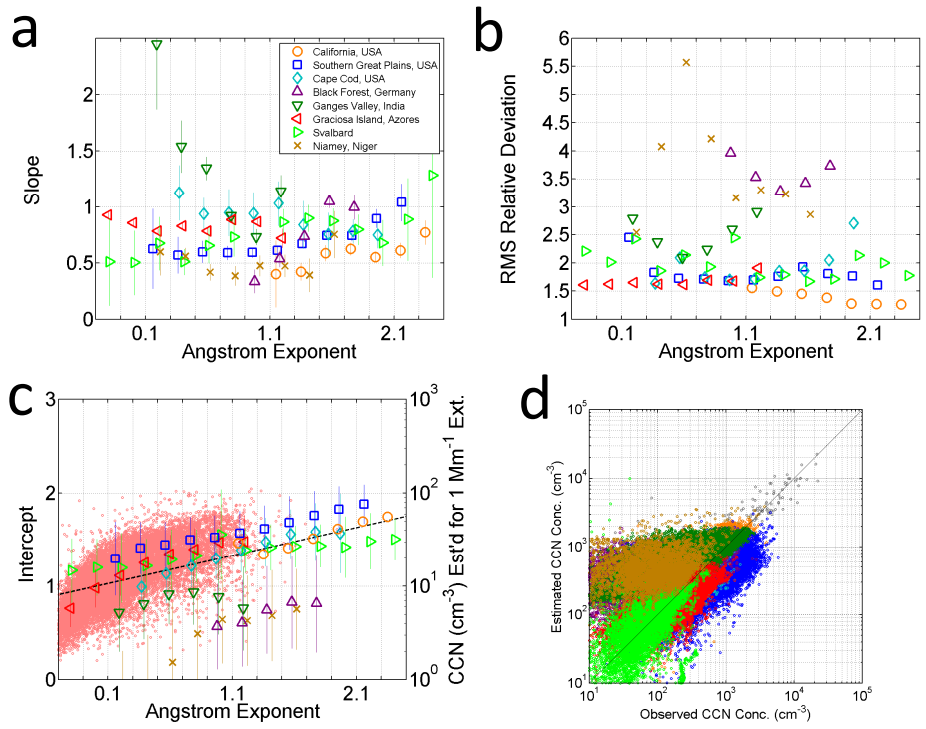

2

3 Figure S3. Same as Figure 3 but for supersaturation of 0.1-0.3% instead of 0.3-0.5%. The
4 RMS difference calculated for all but Niamey data is a factor of 3.0.

5

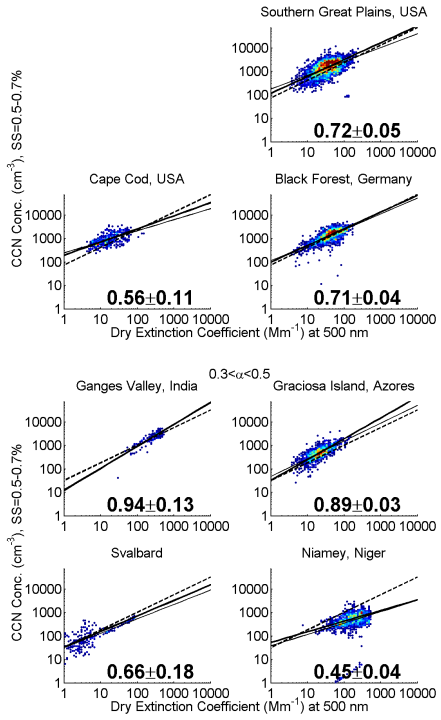

Figure S4. Same as Figure 2 but for supersaturation of 0.5-0.7% instead of 0.3-0.5%.

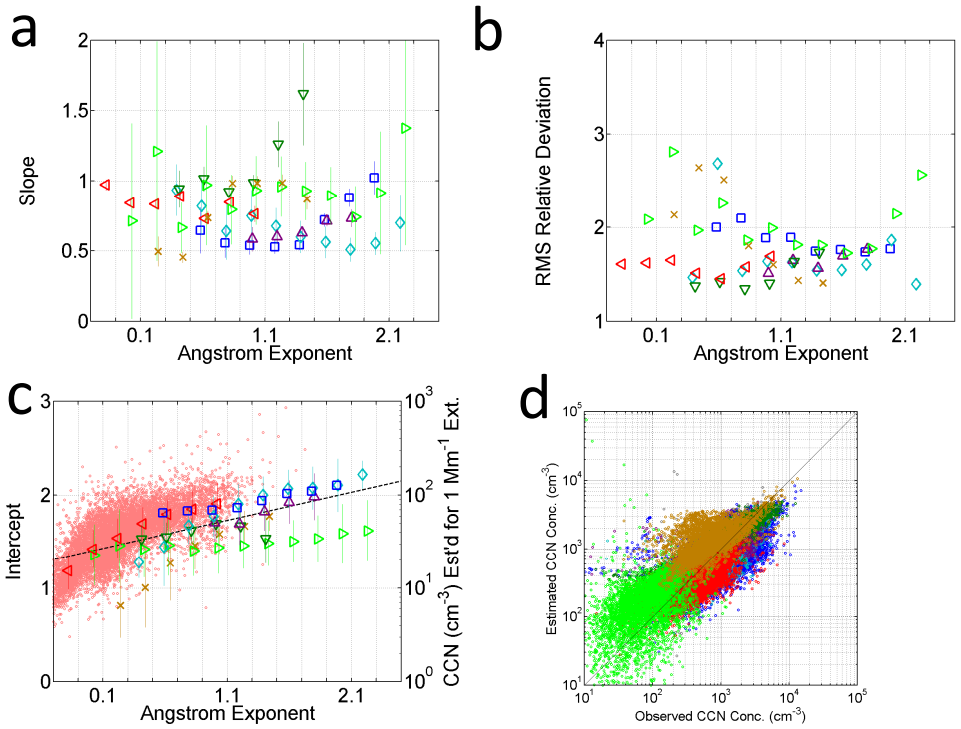

Figure S5. Same as Figure 3 but for supersaturation of 0.5-0.7% instead of 0.3-0.5%. The RMS difference calculated for all but Niamey data is a factor of 2.1.